



# Gene Expression Pattern and Protein Localization of Arabidopsis Phospholipase D Alpha 1 Revealed by Advanced Light-Sheet and Super-Resolution Microscopy

Dominik Novák<sup>1†</sup>, Pavol Vadovič<sup>1†</sup>, Miroslav Ovečka<sup>1</sup>, Olga Šamajová<sup>1</sup>, George Komis<sup>1</sup>, Jean Colcombet<sup>2</sup> and Jozef Šamaj<sup>1\*</sup>

<sup>1</sup> Department of Cell Biology, Centre of the Region Haná for Biotechnological and Agricultural Research, Palacký University Olomouc, Olomouc, Czechia, <sup>2</sup> UMR9213 Institut des Sciences des Plantes de Paris Saclay, Orsay, France

## OPEN ACCESS

### Edited by:

Martin Huelskamp,  
Universität zu Köln, Germany

### Reviewed by:

Qun Zhang,  
Nanjing Agricultural University, China  
Fatima Cvrckova,  
Charles University, Czechia

### \*Correspondence:

Jozef Šamaj  
jozef.samaj@upol.cz

<sup>†</sup>These authors have contributed  
equally to this work.

### Specialty section:

This article was submitted to  
Plant Cell Biology,  
a section of the journal  
Frontiers in Plant Science

**Received:** 15 January 2018

**Accepted:** 06 March 2018

**Published:** 21 March 2018

### Citation:

Novák D, Vadovič P, Ovečka M, Šamajová O, Komis G, Colcombet J and Šamaj J (2018) Gene Expression Pattern and Protein Localization of Arabidopsis Phospholipase D Alpha 1 Revealed by Advanced Light-Sheet and Super-Resolution Microscopy. *Front. Plant Sci.* 9:371. doi: 10.3389/fpls.2018.00371

Phospholipase D alpha 1 (PLD $\alpha$ 1, At3g15730) and its product phosphatidic acid (PA) are involved in a variety of cellular and physiological processes, such as cytoskeletal remodeling, regulation of stomatal closure and opening, as well as biotic and abiotic stress signaling. Here we aimed to study developmental expression patterns and subcellular localization of PLD $\alpha$ 1 in Arabidopsis using advanced microscopy methods such as light-sheet fluorescence microscopy (LSFM) and structured illumination microscopy (SIM). We complemented two knockout *pld $\alpha$ 1* mutants with a YFP-tagged PLD $\alpha$ 1 expressed under the *PLD $\alpha$ 1* native promoter in order to study developmental expression pattern and subcellular localization of PLD $\alpha$ 1 in *Arabidopsis thaliana* under natural conditions. Imaging of tissue-specific and developmentally-regulated localization of YFP-tagged PLD $\alpha$ 1 by LSFM in roots of growing seedlings showed accumulation of PLD $\alpha$ 1-YFP in the root cap and the rhizodermis. Expression of PLD $\alpha$ 1-YFP in the rhizodermis was considerably higher in trichoblasts before and during root hair formation and growth. Thus, PLD $\alpha$ 1-YFP accumulated in emerging root hairs and in the tips of growing root hairs. PLD $\alpha$ 1-YFP showed cytoplasmic subcellular localization in root cap cells and in cells of the root transition zone. In aerial parts of plants PLD $\alpha$ 1-YFP was also localized in the cytoplasm showing enhanced accumulation in the cortical cytoplasmic layer of epidermal non-dividing cells of hypocotyls, leaves, and leaf petioles. However, in dividing cells of root apical meristem and leaf petiole epidermis PLD $\alpha$ 1-YFP was enriched in mitotic spindles and phragmoplasts, as revealed by co-visualization with microtubules. Finally, super-resolution SIM imaging revealed association of PLD $\alpha$ 1-YFP with both microtubules and clathrin-coated vesicles (CCVs) and pits (CCPs). In conclusion, this study shows the developmentally-controlled expression and subcellular localization of PLD $\alpha$ 1 in dividing and non-dividing Arabidopsis cells.

**Keywords:** *Arabidopsis thaliana*, development, localization, light-sheet fluorescence microscopy, microtubules, phospholipase D, At3g15730

## INTRODUCTION

The major function of the phospholipase D (PLD) enzymes is to hydrolyse phospholipids such as phosphatidylcholine, resulting in the production of phosphatidic acid (PA) by transphosphatidylation of water and a free soluble head group, e.g., choline (Munnik and Musgrave, 2001). The *PLD* gene family shows significant expansion in plants, and it is represented by 12 *PLD* genes in *Arabidopsis thaliana*, by comparison to just two in animals and one in yeast (Wang et al., 2012). Plant PLDs are distributed in six subclasses:  $\alpha$ - (with 3 members),  $\beta$ - (with 2 members),  $\gamma$ - (with 3 members),  $\delta$ -,  $\epsilon$ -,  $\zeta$ - (all with 2 members), depending on the protein sequences and enzymatic properties of individual members (Qin and Wang, 2002; Wang, 2005; Bargmann and Munnik, 2006; Hong et al., 2016). All 12 phospholipase D (PLD) isoforms in *Arabidopsis* catalyze the transphosphatidylation of water, thus generating phosphatidic acid having variable signaling roles.

Previously, some PLDs were proposed to play a morphogenetic role linked to microtubules. The relation of PLDs with microtubule organization was directly shown in the case of a tobacco PLD isoform that specifically decorates cortical microtubules (Gardiner et al., 2001) leading to the assumption that PLDs may be a specific component linking cortical microtubules to the cell wall—plasma membrane—cortical cytoskeleton continuum. Later studies on transgenic *Arabidopsis* cell lines using pull-down assay with GFP tagged PLD $\delta$  identified PLD $\delta$  as a cortical microtubule-binding protein (Andreeva et al., 2009; Ho et al., 2009; Hong et al., 2016). Such regulatory interactions among microtubules and PLD isoforms (particularly the *Arabidopsis* PLD $\alpha$ 1 isoform) proved to have functional consequences during plant responses to salt and hyperosmotic stress (Zhang et al., 2012), ABA-induced stomatal closure (Jiang et al., 2014), and drug-induced microtubule reorganization (Zhang et al., 2017a). One prominent target of PLD $\alpha$ 1-produced phosphatidic acid is MAP65-1, a microtubule crosslinker which contains motifs for phosphatidic acid binding outside its carboxylterminal microtubule binding domain (Zhang et al., 2012). Interestingly, phosphatidic acid binding seems to occur at the self-association aminoterminal of MAP65-1. Known and expected new functions of PLD $\alpha$ 1 in plants might link this enzyme to G proteins, cytoskeleton and vesicular trafficking (e.g., Choudhury and Pandey, 2016, 2017; Hong et al., 2016). However, overall regulation of developmental expression pattern in cell- and tissue-specific context and subcellular localization of PLD $\alpha$ 1 in dividing cells is not known.

Dynamic cellular and subcellular changes can be monitored for long periods with light-sheet microscopy. Moreover, imaging can be done at near physiological conditions with minimal phototoxicity at high speed. The method is based on sample illumination with a thin layer of light, thus eliminating out-of-focus excitation and preventing photobleaching. The detection path is oriented orthogonally to the illumination while plant is growing vertically according to gravity vector (Ovečka et al., 2015). Super-resolution microscopy methods can bend or overcome diffraction limitations of conventional microscopes. One such method is structured illumination microscopy (SIM;

Rego et al., 2012). SIM illuminates the sample with a light pattern which combines with diffraction orders of the emitting sample to Moiré patterns. Many such patterns are generated by rotation and phase shifting of the illumination pattern. Individual images taken through high-numerical aperture objectives are combined from each position of the light pattern to reconstruct the final image (Komis et al., 2015).

In this study, we utilized advanced microscopy method such as light-sheet microscopy for developmental imaging of PLD $\alpha$ 1 under natural condition to explore cell-type specific expression. In addition, we provide a high-resolution subcellular localization of PLD $\alpha$ 1 in both dividing and non-dividing *Arabidopsis* cells in the root meristem and leaf petioles.

## MATERIALS AND METHODS

### Plant Material, Mutant Screens

Seedlings were grown vertically on half-strength MS medium (Murashige and Skoog, 1962) supplemented with 0.5% (w/v) gellan gum for 14 d in Fytotron with 21°C and a 16/8 h (light/dark) photoperiod. The illumination intensity was 150  $\mu\text{mol m}^{-2} \text{s}^{-1}$ . Plants 12–15 days old were transferred to soil and cultivated in Fytotron with 21°C and a 16/8 h (light/dark) photoperiod and with the illumination intensity of 150  $\mu\text{mol m}^{-2} \text{s}^{-1}$ .

We have used T-DNA insertion lines *pld $\alpha$ 1-1* (SALK\_067533) and *pld $\alpha$ 1-2* (SALK\_053785) described previously by Bargmann et al. (2009) and Zhang et al. (2004). To check the T-DNA insertions primers were designed by the SIGNAL iSect tool (<http://signal.salk.edu/tdnaprimers.2.html>), and PCR was performed using genomic DNA from seedlings. *A. thaliana* ecotype Columbia-0 (Col-0) was used as the control in the complementation assay (stomatal aperture measurement).

### Preparation of Complemented PLD $\alpha$ 1-YFP

To genetically complement mutant lines, the coding sequence of wild-type *PLD $\alpha$ 1* (At3g15730) along with the native *PLD $\alpha$ 1* promoter (1,944 bp upstream of the initiation codon ATG of *PLD $\alpha$ 1*) was cloned into pGreen0229-YFP-Tnos vector using *Bam*HI-*Kpn*I restriction digest to generate *proPLD $\alpha$ 1::PLD $\alpha$ 1:YFP* construct. The constructs were confirmed by sequencing and transformed by floral dip method (Clough and Bent, 1998; Davis et al., 2009) to *Arabidopsis* Col-0 ecotype (wild type) as well as to *pld $\alpha$ 1-1* and *pld $\alpha$ 1-2* mutants using *Agrobacterium tumefaciens* strain GV 3101. In T1 generation we have selected three independent transgenic lines with the same fluorescent properties. One line was chosen and T2 or T3 progeny of BASTA-resistant transformants, carrying a single homozygous insertion, were used for experiments.

### Preparation of Transgenic Line Carrying PLD $\alpha$ 1-YFP and mRFP-TUB6

*Arabidopsis pld $\alpha$ 1-2* stably expressing *proPLD $\alpha$ 1::PLD $\alpha$ 1:YFP* in T2 generation were crossed with Col-0 plants stably expressing *pUBQ1:mRFP::TUB6* kindly provided by Geoffrey O. Wasteney (Ambrose et al., 2011). F1 generation plants with PLD $\alpha$ 1-YFP and mRFP-TUB6 expression were selected based on fluorescence

signal in the epifluorescence microscope (Axio Imager.M2, Carl Zeiss, Germany).

## Immunoblotting Analysis

Immunoblotting analysis was performed as described previously (Takác et al., 2017). Seedlings of 5 days old *pldα1-1* PLDα1-YFP and *pldα1-2* PLDα1-YFP complemented plants, a progeny from one selected T2 plant from each independent transgenic SALK line, were used for immunoblotting analysis. Roots from ~50 seedlings of 14 days old plants of *A. thaliana*, ecotype Col-0, *pldα1-1*, and *pldα1-2* single mutants as well as *pldα1-1* PLDα1-YFP and *pldα1-2* PLDα1-YFP complemented lines were homogenized using liquid nitrogen to fine powder and the proteins were extracted in E-buffer [50 mM HEPES (pH 7.5), 75 mM NaCl, 1 mM EGTA, 1 mM MgCl<sub>2</sub>, 1 mM NaF, 10% (v/v) glycerol, Complete™ EDTA-free protease inhibitor and PhosSTOP™ phosphatase inhibitor cocktails (both from Roche, Basel, Switzerland)]. After centrifugation at 13000 g in 4°C for 15 min, supernatants were mixed with 4-fold concentrated Laemmli buffer [final concentration 62.5 mM Tris-HCl (pH 6.8), 2% (w/v) SDS, 10% (v/v) glycerol, 300 mM 2-mercaptoethanol] and boiled for 5 min. Protein extracts were separated on 12% TGX Stain-Free™ (Bio-Rad) gels (Biorad). Equal protein amounts were loaded for each sample. Proteins were transferred to polyvinylidene difluoride (PVDF) membranes in a wet tank unit (Bio-Rad) overnight at 24 V and 4°C using the Tris-glycin-methanol transfer buffer. Membranes were blocked in a mixture of 4% (w/v) low-fat dry milk and 4% (w/v) bovine serum albumin in Tris-buffered-saline (TBS, 100 mM Tris-HCl; 150 mM NaCl; pH 7.4) at 4°C overnight. Following washing step with TBS-T (TBS, 0.1% Tween 20) membranes were incubated with polyclonal anti-phospholipase D alpha 1/2 antibody (Agrisera, Sweden) diluted 1:5000 in TBS-T containing 1% (w/v) BSA or with anti-GFP monoclonal antibody (Sigma-Aldrich, Merck, USA) diluted 1:1000 in TBS-T containing 1% (w/v) BSA at room temperature for 1.5 h. As a loading and protein transfer control, membranes were incubated with anti-beta-tubulin monoclonal antibody (Sigma-Aldrich, Merck, USA) diluted 1:2000 in TBS-T containing 1% (w/v) BSA at room temperature for 1.5 h. Following five washing steps in TBST, membranes were incubated 1.5 h at RT with a horseradish peroxidase (HRP) conjugated goat anti-rabbit IgG secondary antibody (diluted 1:5000) in the case of anti-phospholipase D alpha 1/2 primary antibody, and with a HRP conjugated goat anti-mouse IgG secondary antibody (diluted 1:5000; both from Santa Cruz Biotechnology, Santa Cruz, CA, USA) in the case of anti-GFP and anti-beta-tubulin primary monoclonal antibody. After washing in TBS-T, the signals were developed using Clarity Western ECL substrate (Biorad, Hercules, CA, USA). Luminescence was detected on Chemidoc MP documentation system (Biorad). Three biological replicates of immunoblot experiment were performed.

## Stomatal Aperture Measurement

Cotyledons of 7 days-old plants of various genotypes were used for stomatal closure analysis as described previously (Jiang et al.,

2014). Dissected cotyledons were floated on stomatal opening buffer [10 mM 2-(N-morpholino) ethanesulfonic acid (MES-KOH), pH = 6.15 and 30 mM KCl] under light for 2 h to fully open the stomata. Then they were treated with ABA (10 μM) in stomatal opening buffer for indicated period of time. ABA stock solution was prepared in ethanol. Ethanol in stomatal opening buffer was used as a negative control. Final concentration of ethanol in experimental solutions did not exceeded 0.01% (v/v). Stomatal aperture was documented using epifluorescence microscope AxioImager.M2 (Carl Zeiss, Germany) equipped with EC Plan-Neofluar 10x/0.30 objective (Carl Zeiss, Germany) using transmission light in single focal plane and quantitatively analyzed using Fiji (ImageJ) software.

## Whole Mount Immunofluorescence Labeling

Immunolocalization of microtubules, PLDα1, PLDα1-YFP, and clathrin in root wholemounts was done as described previously (Šamajová et al., 2014). Samples were immunolabeled with rat anti-α-tubulin (clone YOL1/34; ABD Serotec), rabbit anti-phospholipase D alpha 1/2 (Agrisera, Sweden), mouse monoclonal anti-clathrin LC (Sigma-Aldrich) or mouse anti-GFP (Abcam) primary antibodies diluted 1:300, 1:300, 1:300 and 1:100, respectively, in 3% (w/v) BSA in PBS at 4°C overnight. In the case of double or triple co-immunolocalization a sequential immunolabeling was performed. Secondary antibodies included Alexa-Fluor 488 goat anti-rat, Alexa-Fluor 488 goat anti-mouse or Alexa-Fluor 546 goat anti-rat IgGs were diluted 1:500 in PBS containing 3% (w/v) BSA for 3 h (1.5 h at 37°C and 1.5 h at room temperature). Where necessary, nuclei were counterstained with DAPI. Microscopic analysis of immunolabeled samples was performed with a Zeiss 710 CLSM platform (Carl Zeiss, Jena, Germany), using excitation lines at 405, 488, and 561 nm from argon, HeNe, diode, and diode pumped solid-state lasers.

## Light-Sheet Fluorescence Microscopy

Developmental live cell imaging of 2–3 days old Arabidopsis plants with PLDα1-YFP expression was done with the light-sheet Z.1 fluorescence microscope (Carl Zeiss, Germany) equipped with W Plan-Apochromat 20x/1.0 NA or W Plan-Apochromat 40x/1.0 NA objectives (Carl Zeiss, Germany) and two LSMF 10x/0.2 NA illumination objectives (Carl Zeiss, Germany). Seedlings were prepared in fluorinated ethylene propylene (FEP) tubes with an inner diameter of 2.8 mm and wall thickness of 0.2 mm (Wolf-Technik, Germany) according to the “open system” protocol for long-term live-cell imaging of *A. thaliana* seedlings described by Ovečka et al. (2015). Root was growing in the block of the culture medium inside of the FEP tube and upper green part of the seedling developed in an open space of the FEP tube with the access to air. Sample holder with the sample was placed into observation chamber of the light-sheet microscope tempered to 22°C using a Peltier heating/cooling system. Before insertion of the sample to the microscope plants were ejected slightly out of the FEP tube allowing imaging of the root in the block of solidified culture medium, but without the FEP tube. Before the imaging, liquid medium filling the observation chamber was filter-sterilized using a sterile syringe

filter. Roots were imaged using dual-side light-sheet illumination with excitation laser line 514 nm, beam splitter LP 580 and with emission filter BP525-565. Images were recorded with the PCO.Edge sCMOS camera (PCO AG, Germany) with the exposure time 30 ms and the imaging frequency of every 5 min in Z-stack mode for 5–20 h. Scaling of recorded images in x, y, and z dimensions was  $0.228 \times 0.228 \times 0.499 \mu\text{m}$ . For counterstaining of plant cell walls with propidium iodide, seedlings were germinating and growing in blocks of the solidified culture medium containing  $1 \mu\text{g}\cdot\text{ml}^{-1}$  of propidium iodide (Invitrogen, USA) before imaging. Seedlings (2 days old) growing directly in the solidified medium containing propidium iodide were transferred to the light-sheet microscope for root imaging.

### Spinning Disk and Confocal Laser Scanning Microscopy

Hypocotyls, leaves with pavement cells, stomata, and trichomes of 5–8 DAG Arabidopsis plants with PLD $\alpha$ 1-YFP expression were documented with spinning disk microscope (Cell Observer SD, Carl Zeiss, Germany) equipped with Plan-Apochromat 20x/0.8 (Carl Zeiss, Germany) and Plan-Apochromat 63x/1.40 Oil (Carl Zeiss, Germany) objectives. Cells were imaged with excitation laser 514 nm and with emission filter BP535/30 for YFP. Cotyledons, petioles and guard cells were documented with confocal laser scanning microscope LSM 710 (Carl Zeiss, Germany) equipped with Plan-Apochromat 20x/0.8 (Carl Zeiss, Germany) and alpha Plan-Apochromat 63x/1.46 Oil (Carl Zeiss, Germany) objectives. Plants of 6 DAG were stained with  $4 \mu\text{M}$  FM4-64 (Invitrogen, USA) diluted in half-strength liquid MS medium for 90 min before imaging. Samples were imaged with excitation lasers 514 nm for YFP and 561 nm for mRFP and FM4-64, beam splitters MBS 458/514 for YFP, MBS 458/561 for mRFP and MBS 488/561 for FM4-64. Emission spectrum used were 519–550 nm for YFP, 590–610 nm for mRFP and 651–759 nm for FM4-64.

### Structured Illumination Microscopy

The same immunolabeled wholemount samples examined with CLSM were also analyzed via a Zeiss SIM platform coupled with a PCO.Edge 5.5 sCMOS camera (Elyra PS.1, Carl Zeiss, Germany). Fluorophores were excited with the 405, 488, 561, and 647 nm laser lines. For acquisition with a 63x/1.40 oil immersion objective, the grating pattern was set to 5 rotations with 5 standard phase shifts per angular position. In case of Z-stacks, Nyquist sampling was selected to be the smallest one (corresponding to DAPI channel with 91 nm section thickness), leading to oversampling of the rest of the channels. Image reconstruction was done according to previously published procedures (Komis et al., 2015).

### Image Processing

The post-processing, default deconvolution using Nearest Neighbour or Constrained Iterative algorithms and profile measurement of all fluorescence images in this study, including 3D reconstruction or maximum intensity projection from individual z-stacks and creating subsets was done using ZEN 2010 software. All images exported from ZEN 2010 software

were assembled and captioned in Microsoft PowerPoint to final figures.

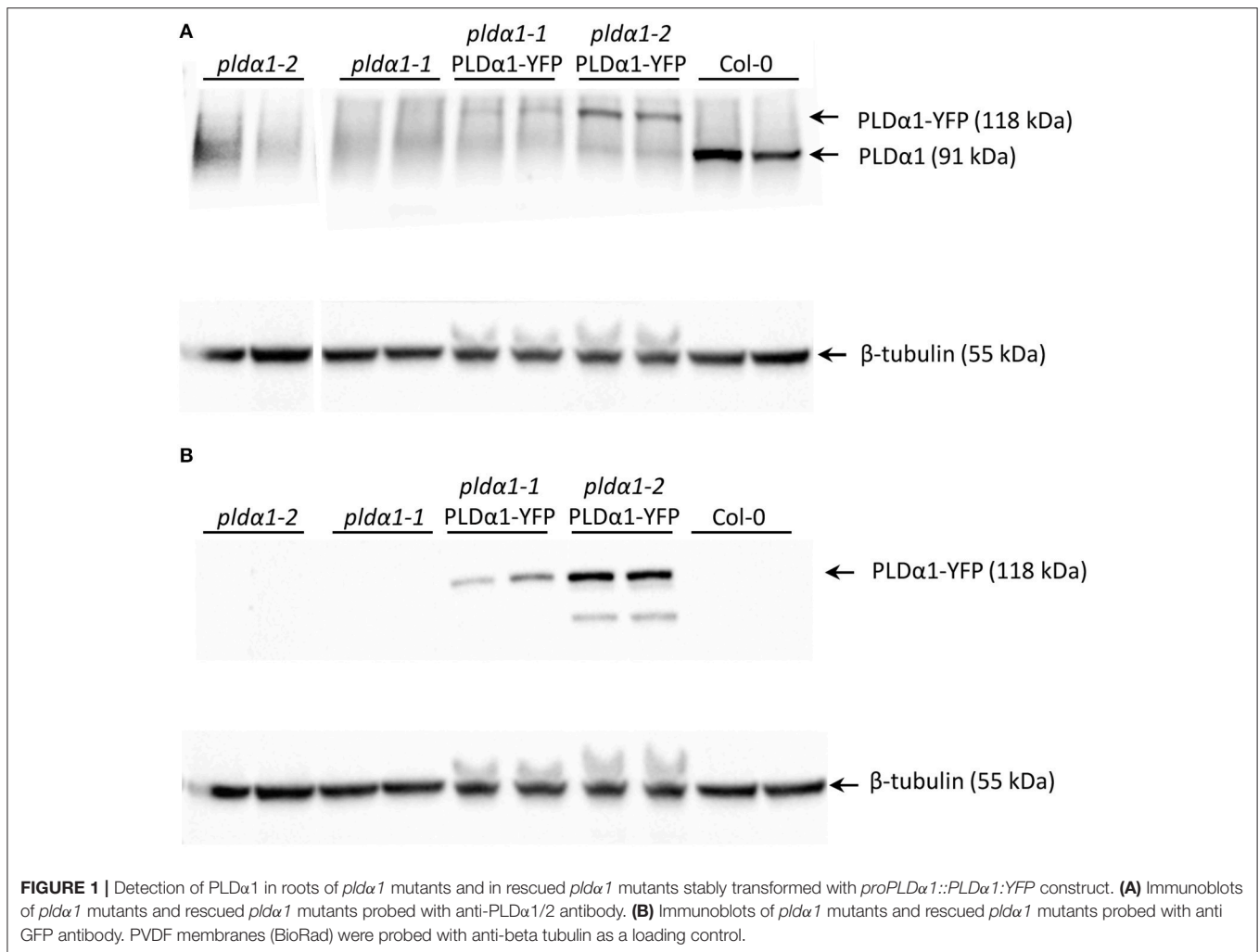
## RESULTS

### Expression Patterns of PLD $\alpha$ 1-YFP in Arabidopsis Plants

In order to characterize the roles of PLD $\alpha$ 1 in plant development, we performed *in vivo* cell- and tissue-specific expression analysis of the PLD $\alpha$ 1-YFP driven by native *PLD $\alpha$ 1* promoter in two stably transformed *pld $\alpha$ 1* mutants of *A. thaliana*. Thus, both *pld $\alpha$ 1-1* and *pld $\alpha$ 1-2* mutants were stably transformed with *proPLD $\alpha$ 1::PLD $\alpha$ 1:YFP* construct using the floral dip method (Clough and Bent, 1998). Comparison of *proPLD $\alpha$ 1::PLD $\alpha$ 1:YFP* expression patterns in different aerial organs and tissues of *pld $\alpha$ 1-1* and *pld $\alpha$ 1-2* mutants stably expressing PLD $\alpha$ 1-YFP is presented in **Figure S1**. To prove the expression of PLD $\alpha$ 1-YFP fusion protein in experimental plants (*pld $\alpha$ 1-1* and *pld $\alpha$ 1-2* mutant plants stably transformed with *proPLD $\alpha$ 1::PLD $\alpha$ 1:YFP* construct), we performed SDS-PAGE with immunoblot analysis using anti-phospholipase D alpha 1/2 and anti-GFP antibodies. This analysis confirmed the presence of PLD $\alpha$ 1-YFP fusion protein with the expected molecular mass of 118 kDa, using both anti-PLD $\alpha$ 1 and anti-GFP antibodies (**Figures 1A,B**). In Col-0, which was used as a control, anti-PLD $\alpha$ 1 antibody showed a protein band with a molecular mass of 91.8 kDa corresponding to PLD $\alpha$ 1. We also confirmed the absence of PLD $\alpha$ 1 protein in both *pld $\alpha$ 1-1* and *pld $\alpha$ 1-2* mutant plants. In addition, Col-0, *pld $\alpha$ 1-1*, and *pld $\alpha$ 1-2* mutant plants were used as negative controls for the use of the anti-GFP antibody and we did not observe any band in these lines (**Figure 1B**).

### Functional Complementation of *pld $\alpha$ 1-1* and *pld $\alpha$ 1-2* Mutants With PLD $\alpha$ 1-YFP Expression Driven Under Its Own Promoter

Cellular levels of abscisic acid (ABA) increase in responses to drought and salt stresses, which promotes stomatal closure in order to prevent water loss. Although PLD $\alpha$ 1 is the most predominant PLD in plants, *pld $\alpha$ 1* knockout mutants do not exhibit significant phenotypical changes (Fan et al., 1997; Zhang et al., 2012). Nevertheless, PLD $\alpha$ 1 controls proper water balance in plants responding to ABA by stomatal closure and this response is impaired in the *pld $\alpha$ 1* knockout mutants (Jiang et al., 2014; Pleskot et al., 2014; Zhang et al., 2017a). To verify that *pld $\alpha$ 1-1* and *pld $\alpha$ 1-2* mutants were complemented with *proPLD $\alpha$ 1::PLD $\alpha$ 1:YFP* construct and show wild type-like behavior, we examined stomatal closure ability of these revertants by measuring stomatal aperture in cotyledons of 7 days old plants after treatment with  $10 \mu\text{M}$  ABA. We have observed significantly increased stomatal closure after ABA treatment of wild type plants in comparison to *pld $\alpha$ 1-1* and *pld $\alpha$ 1-2* mutants, which were ABA-insensitive and showed no change in stomatal apertures (**Figure 2**). These results were consistent with published data (Zhang et al., 2004; Jiang et al., 2014). Importantly, *pld $\alpha$ 1-1* and *pld $\alpha$ 1-2* mutant plants genetically complemented with *proPLD $\alpha$ 1::PLD $\alpha$ 1:YFP* construct reacted



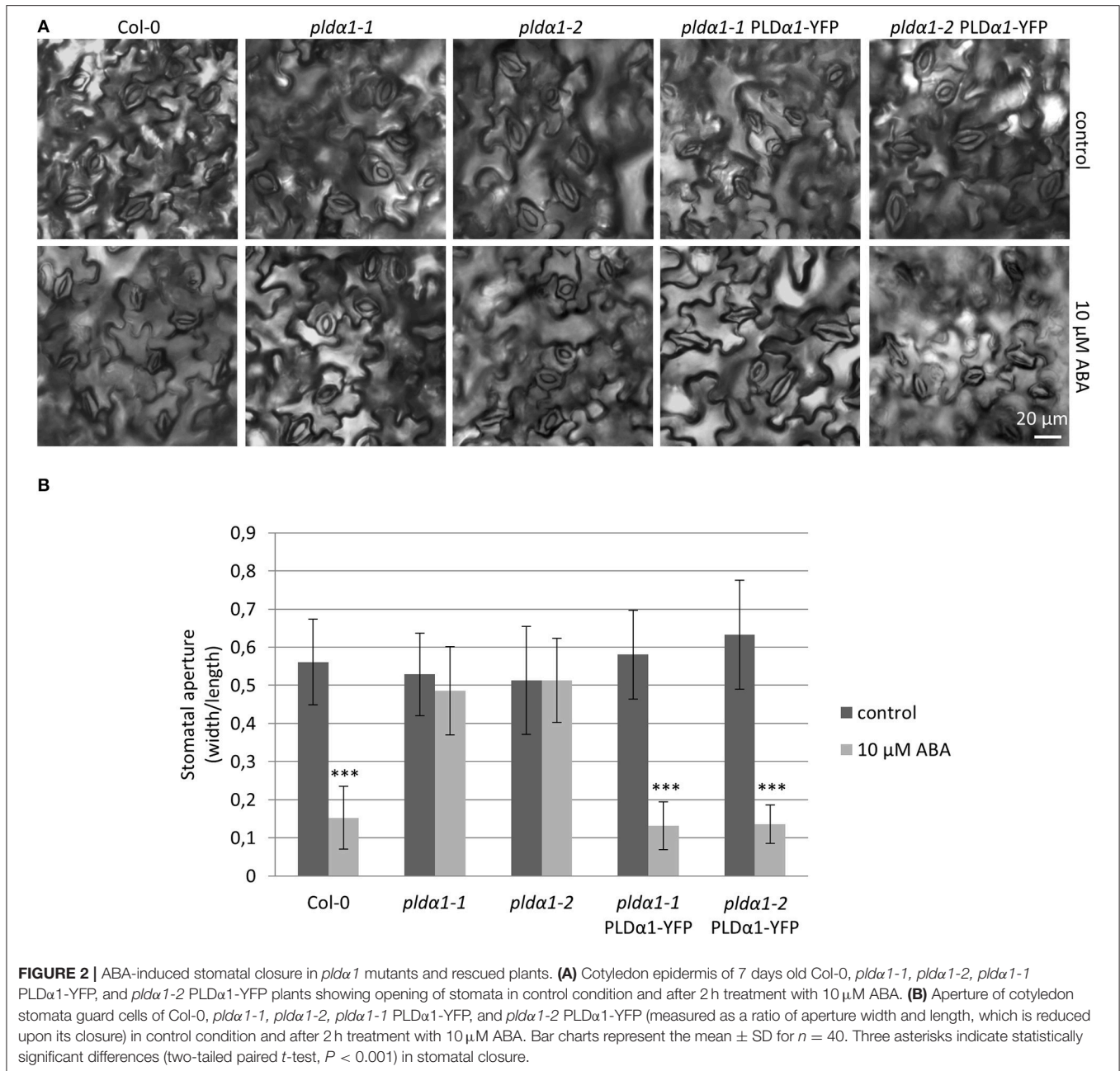
to ABA treatment by substantial decrease of stomatal aperture, similarly to the wild type plants (**Figure 2**). These results confirmed the phenotypical complementation of *pldα1-1* and *pldα1-2* mutants with *proPLDα1::PLDα1:YFP* construct which can be considered as a functional one for further expression and localization studies.

## Developmental Expression Pattern and Localization of PLDα1-YFP in Arabidopsis Plants

Observation of developmental expression pattern and localization of PLDα1-YFP fusion protein has been done in *pldα1-1* mutant stably expressing a *proPLDα1::PLDα1:YFP* construct at cell-, tissue- and organ-specific levels using light-sheet fluorescence microscopy (LSFM). Subcellular localization was performed using confocal and spinning disk microscopy. Developmental LSFM has been performed with 2- to 3-days old seedlings that were growing inside of the microscope imaging chamber in time periods ranging from 5 to 20 h. During these imaging periods, roots of experimental plants exhibited

continuous growth at constant root growth rates. LSFM offered the possibility not only to localize PLDα1-YFP at the cellular level in root surface tissues (**Figure 3A**), but it also allowed deep root imaging and tissue-specific visualization and localization of PLDα1-YFP in internal root tissues (**Figure 3B**, **Figures S2, S3**).

Imaging of tissue-specific expression of PLDα1-YFP in roots using LSFM revealed developmental regulation of PLDα1-YFP amount in the root apex. The expression levels of PLDα1-YFP in the root meristematic zone including rhizodermis, cortex, and procambium were relatively low (**Figure 3B**). On the other hand, particularly strong expression levels were revealed in the apical and lateral root cap cells (**Figure 3C**). Remarkably strong expression was observed in central columella cells and particularly in cells of the third columella layer (**Figures 3B,C**). Semi quantitative evaluation of the PLDα1-YFP amount in different cell layers of root apex (**Figure 3D**) revealed a steep gradient between third and fourth outermost layers of the central root cap (**Figures 3D–F**; profiles 1–2). There was a relatively low amount of PLDα1-YFP in the primary meristems at the position of the stem cell niche in comparison to the lateral root cap cells (**Figures 3D–F**; profile 3). Proximally to the region of initial cells



there was a clear gradient in the PLDα1-YFP amount within the radial organization of the root meristem with the highest level in the lateral root cap cells, much lower level in the rhizodermis, cortex and endodermis, and the lowest level in central cylinder tissues (Figures 3D–F; profile 4). Different expression levels among lateral root cap cells, dermal tissues (rhizodermis, cortex, and endodermis) and central cylinder tissues were clearly visible in the central part of the root meristematic zone (Figures 3D–F; profile 5).

In comparison to the relatively low expression level of the PLDα1-YFP in the root meristem, a dramatic enhancement was detected in the root transition zone, particularly in

the rhizodermis (Figure 4A). Rhizodermal cells showed much stronger expression levels in the trichoblast cell files compared to the atrichoblast ones (Figures 4B–E). The relatively strong expression of PLDα1-YFP in trichoblast cells of the transition root zone revealed one additional aspect of particular interest. It was the strongly polarized localization of PLDα1-YFP at the cell corner of the trichoblasts facing the cleft contact with two underlying cortical cells (Figures 4A,C). Thereon, the strong expression levels of PLDα1-YFP in trichoblast cell files was also maintained later in the development of root hairs during bulge formation (Figure 4B) and in tip-growing root hairs (Figures 4F–H). Time-course semi quantitative evaluation

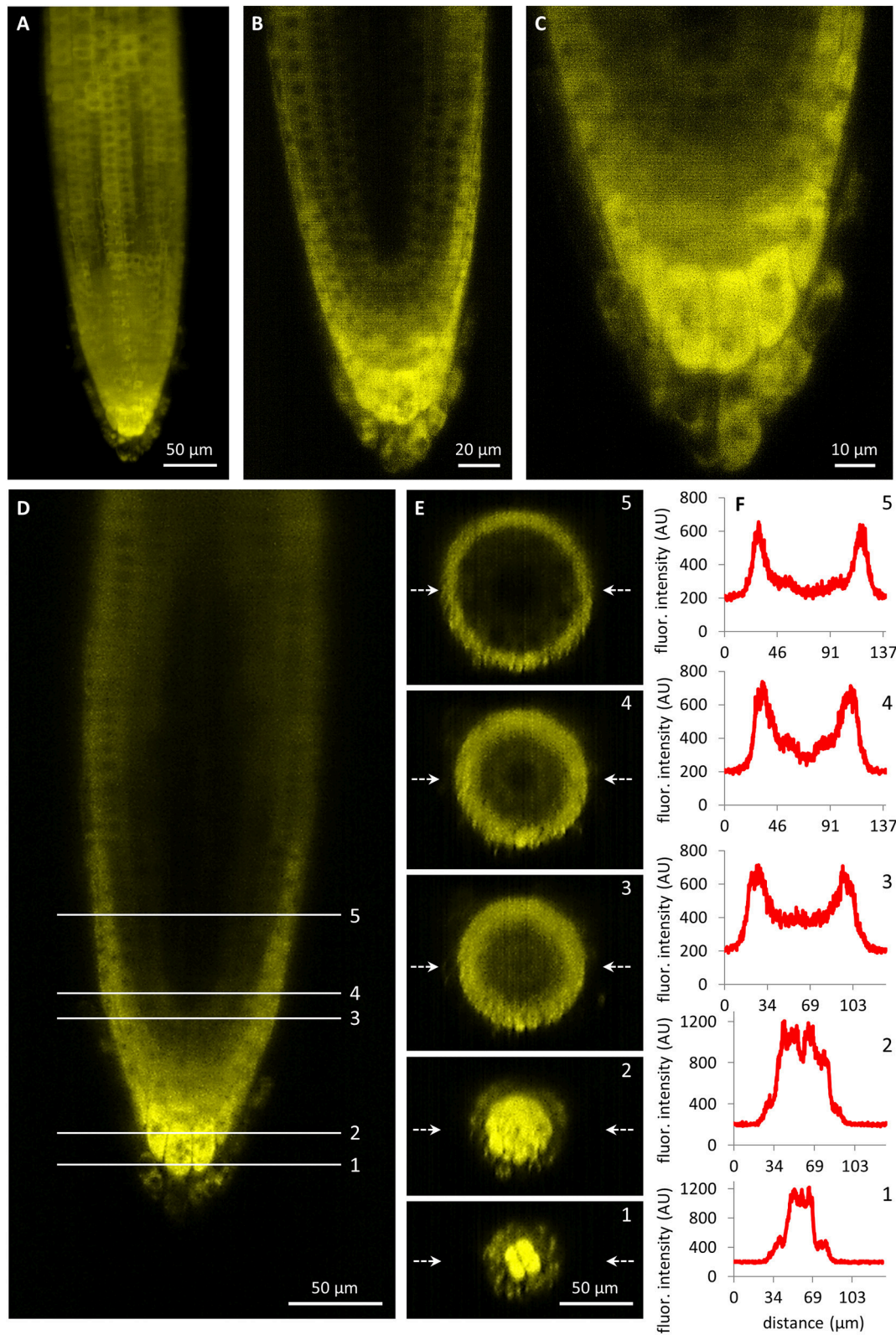


**FIGURE 3 |** Light-sheet fluorescence microscopy localization of PLD $\alpha$ 1-YFP driven by *PLD $\alpha$ 1* own promoter in *Arabidopsis thaliana* roots. **(A)** Overview of PLD $\alpha$ 1-YFP localization in different tissues of the root tip constructed from maximum intensity projection of 330 optical sections (with thickness of 0.5  $\mu$ m each). *(Continued)*

**FIGURE 3** | The amount of PLD $\alpha$ 1-YFP fluctuated in root rhizodermal cells while the highest localization was visible in the root cap cells. **(B)** Median optical section of the root tip revealed differential distribution of PLD $\alpha$ 1-YFP with the strongest expression in the root cap and lateral root cap cells and with much lower production of PLD $\alpha$ 1-YFP in rhizodermal, cortical and endodermal cell layers and with very low production in procambial cells. **(C)** Detail of the root cap showing the strongest expression level of PLD $\alpha$ 1-YFP in central columella cells and particularly in cells of the third root cap layer. **(D–F)** Qualitative and semi-quantitative evaluation of the relative PLD $\alpha$ 1-YFP distribution in longitudinal and radial zonation of the root tip. Five profiles at different positions of the root tip **(D)** were visualized into orthogonal projections of radial root sections **(E)** and profiles in the median positions of the radial root sections (indicated by arrows) were quantitatively displayed **(F)**. Images were taken from *pld $\alpha$ 1-1* mutant plants stably expressing PLD $\alpha$ 1-YFP.

of PLD $\alpha$ 1-YFP distribution clearly revealed its accumulation in growing tips of root hairs (**Figures 4G,H**). The PLD $\alpha$ 1-YFP expression pattern in growing roots thus reflected the tissue-specific and developmentally-regulated transition from low PLD $\alpha$ 1-YFP protein levels in actively dividing cells of the root apical meristem to much enhanced protein accumulation in the root transition zone harboring post-mitotic cells preparing for cell elongation (**Figures 3D–F**). Cell differentiation in root tissues led to localized accumulation of PLD $\alpha$ 1-YFP, particularly in the developing rhizodermis, where PLD $\alpha$ 1-YFP accumulated preferentially in trichoblasts (**Figures 4B–E**), especially during the process of root hair formation (**Figures 4F–H**). In all root tissues expressing moderate levels of PLD $\alpha$ 1-YFP (root cap cells, root transition zone, trichoblast cell files and tip growing root hairs) we observed cytoplasmic localization of the fusion protein.

To better identify cell margins and cell types, roots were counterstained with propidium iodide (PI). Although seedling treatment with PI might affect rates of root growth and elongation, expression patterns of PLD $\alpha$ 1-YFP in diverse root tissues and cell types were the same as described above (**Figures S2–S5**).

Expression pattern and localization of PLD $\alpha$ 1-YFP in different cell types of aerial parts of 6 days old seedlings were documented with confocal and spinning disk microscopy. Relatively high expression level of PLD $\alpha$ 1-YFP was observed in hypocotyl epidermal cells (**Figure 5A**), in pavement cells and stomata guard cells of cotyledons (**Figure 5B**), in leaf epidermis and stomata guard cells of leaves (**Figures 5C,D**). Consistently with strong expression level of PLD $\alpha$ 1-YFP in rhizodermis and in developing root hairs we observed also strong expression of PLD $\alpha$ 1-YFP in leaf trichomes (**Figure 5E**). In more detail, high amounts of PLD $\alpha$ 1-YFP were found at tips of trichome branches (**Figure 5E**). A high level of PLD $\alpha$ 1-YFP was observed also in epidermal cells of leaf petioles (**Figure 5F**).

In cells of all examined aerial tissues, PLD $\alpha$ 1-YFP was localized in the cytosol and predominantly at the cell cortex in the vicinity of the plasma membrane. Additionally, PLD $\alpha$ 1-YFP was localized in cytoplasmic strands of interphase cells (**Figure 5F**). Immunofluorescence localization of PLD $\alpha$ 1 protein in root meristematic cells of wild type Col-0 plants using anti-PLD $\alpha$ 1/2 antibody confirmed its homogeneous localization in the cytosol (**Figure S6**).

Accumulation of PLD $\alpha$ 1-YFP in growing root hairs (**Figures 4F–H**) suggested its role in actively growing cell domains. To test this possible scenario in leaf trichomes, we identified individual stages of trichome development in the first true leaf and we performed semiquantitative evaluation of PLD $\alpha$ 1-YFP distribution along single profiles in individual

trichome branches. To quantify PLD $\alpha$ 1-YFP developmental redistribution during trichome formation, we measured profiles of PLD $\alpha$ 1-YFP fluorescence in young trichome primordia without branches (**Figure 6A**), in each individual branch of growing trichomes during later developmental stages (**Figures 6B–D**) up to final stage of fully developed three-branched trichomes (**Figure 6E**). Profiling of fluorescence intensity along individual trichome branches clearly revealed higher accumulation of PLD $\alpha$ 1-YFP at the tip of actually growing branch during trichome development (**Figure 6F**).

### Association of PLD $\alpha$ 1-YFP With Microtubules

In order to investigate the localization of PLD $\alpha$ 1-YFP fusion protein in respect to cortical and mitotic microtubules we crossed *plda-1-2* mutant plants stably expressing *proPLD $\alpha$ 1::PLD $\alpha$ 1:YFP* construct with Col-0 plants stably expressing *pUBQ1::mRFP:TUB6* construct (red fluorescent protein marker fused to Arabidopsis  $\alpha$ -tubulin 6 isoform, Ambrose et al., 2011). Labeling of the plasma membrane in cells of such crossed line was performed with FM4-64. The co-localization experiments were done in non-dividing leaf petiole epidermal cells using confocal laser scanning microscopy (**Figure 7**). 3-D rendering and orthogonal projections showed very close association of cortical microtubules with the plasma membrane and predominant localization of PLD $\alpha$ 1-YFP in the cortical cytoplasm (**Figure 7A**). Merge image of all three markers (**Figure 7A**) and semi-quantitative measurement of fluorescence intensities along transversal profile in the cell cortex (**Figure 7B**) revealed only poor co-localization, but rather association of PLD $\alpha$ 1-YFP with cortical microtubules. This was evident also from spatial separation of individual optical sections from 3-D scans of the cell cortex starting from the cell surface. By taking individual optical sections of 420 nm thickness (**Figure 7C**), we observed uppermost signal of the FM4-64 related to the plasma membrane first, followed by mRFP signal corresponding to cortical microtubules located beneath the plasma membrane, and only then first appearance of the YFP signal related to the PLD $\alpha$ 1. In merge image, the plasma membrane signal was enriched in second and third optical section (0.000 to  $-0.853 \mu\text{m}$  from the cell surface), network of cortical microtubules was present in third to fifth optical section ( $-0.853$  to  $-1.705 \mu\text{m}$  from the cell surface), while PLD $\alpha$ 1-YFP signal was enriched only in fourth to sixth optical section ( $-1.279$  to  $-2.131 \mu\text{m}$  from the cell surface). Association and partial colocalization of PLD $\alpha$ 1-YFP with cortical microtubules (detected as yellow spots in merge images) is visible only on the cytoplasmic face (**Figure 7C**, optical section  $-1.279$ ), but not on



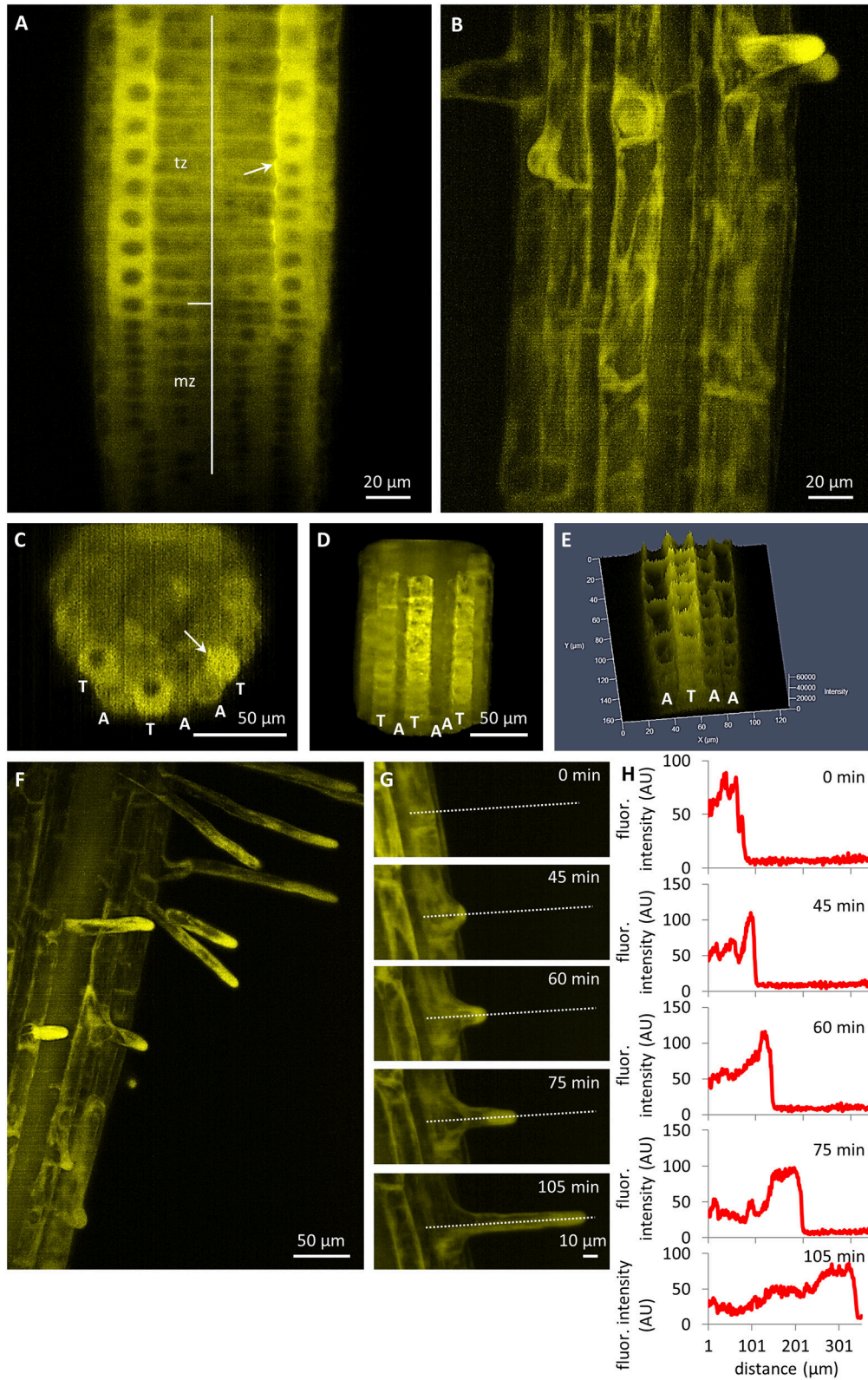


**FIGURE 4** | Tissue- and cell-specific localization of PLD $\alpha$ 1-YFP driven by its own native promoter in the root of *Arabidopsis thaliana* by light-sheet fluorescence microscopy. **(A)** Distribution of PLD $\alpha$ 1-YFP in meristematic zone (mz) with relatively low expression and in transition zone (tz) with enhanced expression.

(Continued)

**FIGURE 4 | (B)** Differentiation zone of the root with stronger expression level of PLD $\alpha$ 1-YFP in trichoblasts and bulges of emerging root hairs and lower expression level in atrichoblast cell files. **(C–E)** Orthogonal projection **(C)**, 3D-rendering **(D)** and intensity-based 3D visualization **(E)** of root differentiation zone showing higher expression level of PLD $\alpha$ 1-YFP in rhizodermal trichoblast cell files (labeled as T) and lower expression level in atrichoblast cell files (labeled as A). Arrows in **(A,C)** point local accumulation of PLD $\alpha$ 1-YFP at the cell corner of the trichoblasts in the contact with two underlying cortical cells. **(F)** Enhanced localization of PLD $\alpha$ 1-YFP in trichoblast cells at the stage of root hair formation and apparent accumulation of PLD $\alpha$ 1-YFP in growing root hairs. **(G)** Time-course recording of accumulation and relocation of PLD $\alpha$ 1-YFP during the root hair outgrowth in trichoblast root cell. Time frames of individual developmental stages are indicated in min. Dotted lines along the median longitudinal axis of the root hair indicate the position of fluorescence intensity profile measurement. **(H)** Fluorescence intensity profiles of PLD $\alpha$ 1-YFP distribution corresponding to particular developmental stages of the root hair formation from the trichoblast root cell in **(G)**. Images were taken from *pld $\alpha$ 1-1* mutant plants stably expressing PLD $\alpha$ 1-YFP using light-sheet microscopy.

the membrane face (**Figure 7C**, optical section  $-0.853$ ) of the cortical microtubule network. Sandwich-like arrangement of the plasma membrane, cortical microtubule network, and PLD $\alpha$ 1-YFP was evident also from orthogonal view of the examined cell cortex area (**Figure 7D**), proven also by semiquantitative fluorescence profile intensity measurement (**Figure 7E**). These experiments revealed predominantly cytoplasmic localization of PLD $\alpha$ 1-YFP.

### Colocalization of PLD $\alpha$ 1-YFP With Microtubules in Dividing Cells

Colocalization of PLD $\alpha$ 1-YFP with mitotic microtubule arrays was observed in dividing epidermal cells of leaf petioles using spinning disk microscopy (**Figures 8A–E**). Association of PLD $\alpha$ 1-YFP with the pre-prophase band of microtubules (PPB) was evident in the pre-prophase and prophase stage (**Figure 8A**), with mitotic spindle during metaphase to anaphase (**Figures 8B–D**) and with progressing phragmoplast during cytokinesis (**Figure 8E**). In the pre-prophase and prophase stage PLD $\alpha$ 1-YFP accumulated in the cell cortex in a ring-like structure that was broader as PPB. This indicates that PLD $\alpha$ 1-YFP, in addition to its colocalization with microtubules inside the PPB, also surrounded PPB in the cortical cytoplasm (**Figures 8A, 9A**). Additionally, PLD $\alpha$ 1-YFP was enriched also in cytoplasmic disk radiating from the nuclear surface to the cell cortex at the PPB plane (**Figure 9A, Video S1**). Later on, PLD $\alpha$ 1-YFP was strongly accumulated in microtubule arrays of the mitotic spindle which was surrounded by cytoplasmic layer enriched with PLD $\alpha$ 1-YFP (**Figures 8B,C**). Association of PLD $\alpha$ 1-YFP with microtubules was documented by missing signal in the mitotic spindle occupied by chromosomes during metaphase and anaphase (**Figures 8B–D**). Starting with the segregation of sister chromatids and their pulling to the opposite spindle poles, PLD $\alpha$ 1-YFP accumulated also in the central zone of the anaphase spindle (**Figures 8C,D**). Appearance of the early phragmoplast was connected with accumulation of PLD $\alpha$ 1-YFP (**Figure 8D**). However, PLD $\alpha$ 1-YFP was absent in the late phragmoplast mid-zone during cell plate formation in cytokinesis (**Figure 8E**). In addition, PLD $\alpha$ 1-YFP was accumulated also in surrounding cytoplasm (phragmosome) enclosing cytokinetic apparatus in the center of partially vacuolated cells (**Figures 8E, 9B, Video S2**). As the late phragmoplast reached the cell periphery, PLD $\alpha$ 1-YFP was associated with emerging cell plate in the central zone of the ring phragmoplast (**Figure 9B, Video S2**). Visual comparison of PLD $\alpha$ 1-YFP protein level in cortical cytoplasm between dividing cells and neighboring non-dividing

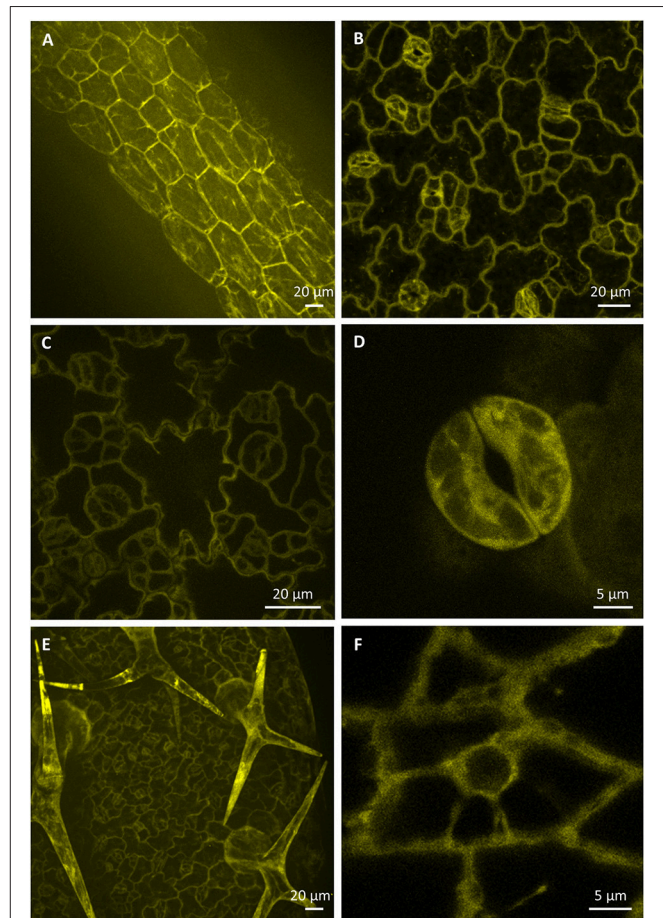
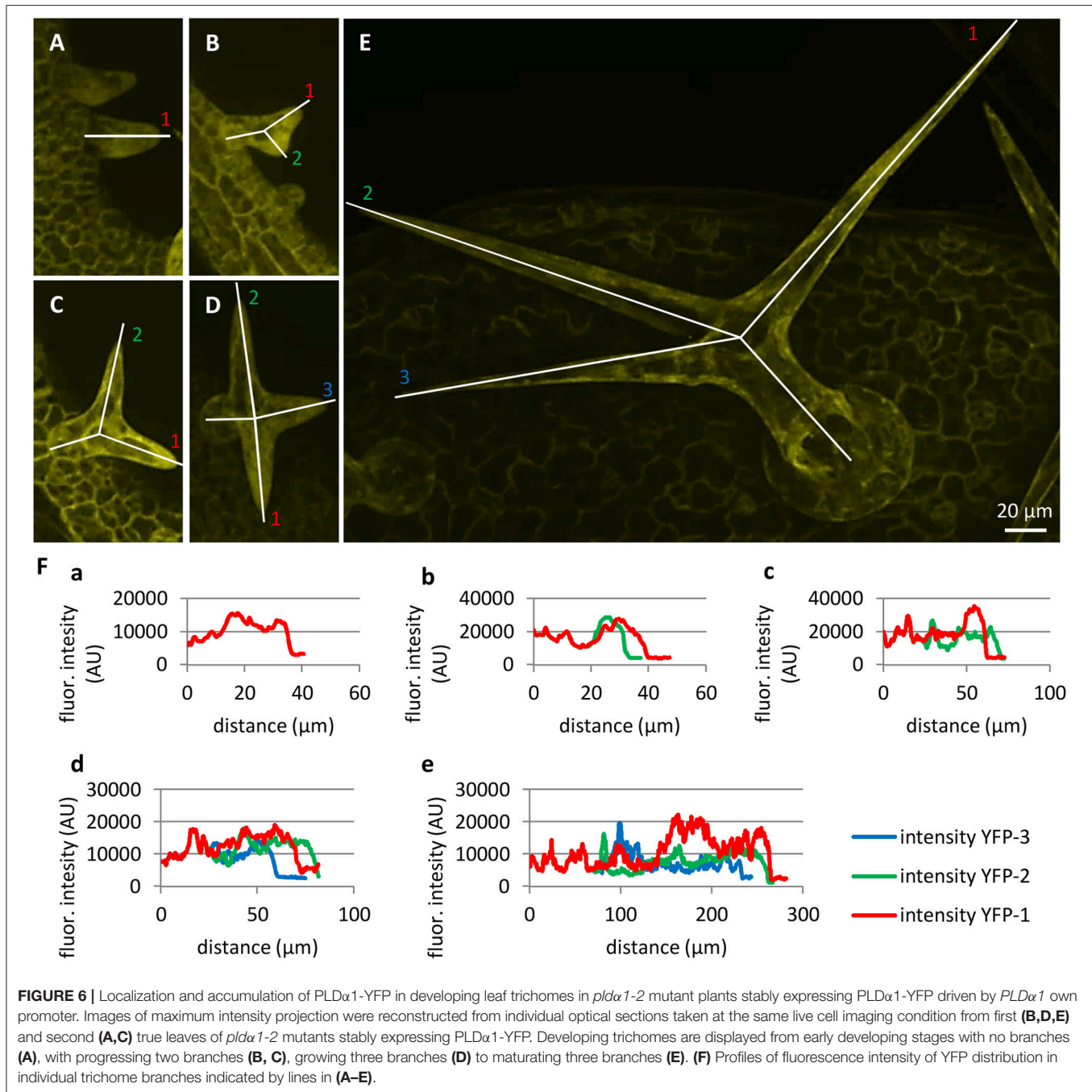


**FIGURE 5 |** Localization of PLD $\alpha$ 1-YFP driven by *PLD $\alpha$ 1* own promoter in different aerial organs and tissues of *Arabidopsis thaliana* seedlings. Images were taken from different cell types of aerial tissues of living *pld $\alpha$ 1-2* mutants stably expressing PLD $\alpha$ 1-YFP driven by its own promoter using confocal and spinning disk microscopy. Localization of PLD $\alpha$ 1-YFP in hypocotyl epidermal cells **(A)**, cotyledon epidermal cells and stomata **(B)**, leaf epidermal pavement cells and stomata guard cells **(C)**, leaf stoma guard cells **(D)**, leaf epidermal cells and trichomes **(E)**, and petiole epidermal cell **(F)**. Spinning disk microscopy **(A,C,D)**, confocal microscopy **(B,E,F)**.

cells (**Figures 8A,E**) clearly indicated intracellular relocation and accumulation of PLD $\alpha$ 1-YFP within and around mitotic microtubule arrays. It indicates potential cell cycle-dependent cooperation of PLD $\alpha$ 1-YFP with microtubules in proliferating cells.



Association of PLD $\alpha$ 1-YFP with mitotic microtubule arrays was confirmed using immunofluorescence colocalization of PLD $\alpha$ 1-YFP and microtubules in root meristem cells of complemented *pld $\alpha$ 1-1* mutant seedlings expressing *proPLD $\alpha$ 1::PLD $\alpha$ 1:YFP* construct. In non-dividing interphase or pre-mitotic cells PLD $\alpha$ 1-YFP protein was localized in the cytoplasm, showing rather homogeneous distribution (**Figure 10A**). However, accumulation as well as partial association of PLD $\alpha$ 1-YFP signal with microtubules of PPB, spindle and both early and late phragmoplast was observed in

mitotic root cells (**Figure 10A**). Detailed analysis of PLD $\alpha$ 1-YFP distribution during cytokinesis revealed its specific association with progressing phragmoplast. 3-D reconstruction, orthogonal projection and rotation of disk phragmoplast with initiated depolymerisation of microtubules in the central part showed predominant association of PLD $\alpha$ 1-YFP with leading (outer) edge of the phragmoplast as well as with the trailing (inner) edge, which was created in the central part of the phragmoplast (**Figure 10B, Video S3**). Accumulation of PLD $\alpha$ 1-YFP at the trailing edge of the late ring phragmoplast was more evident

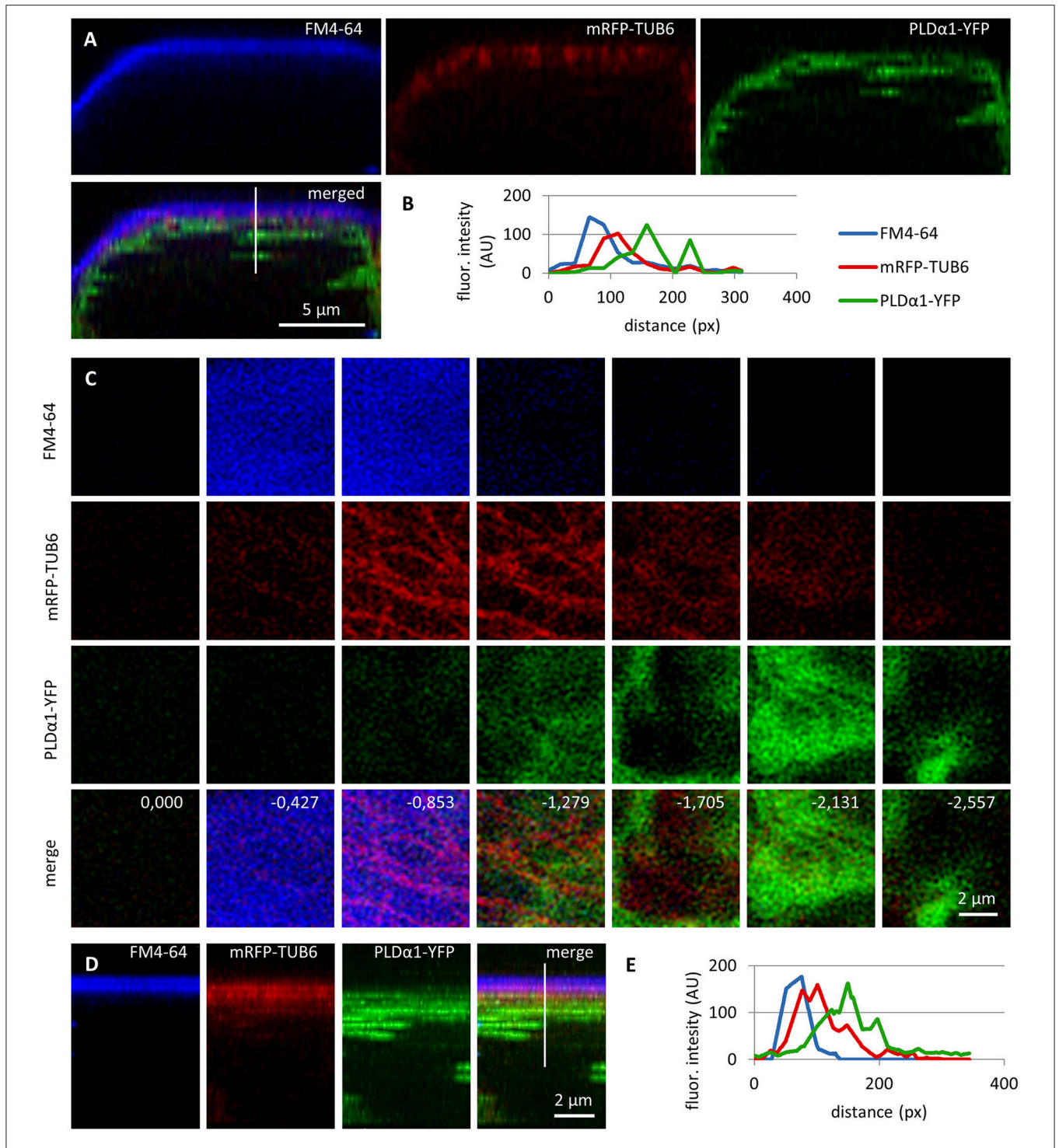
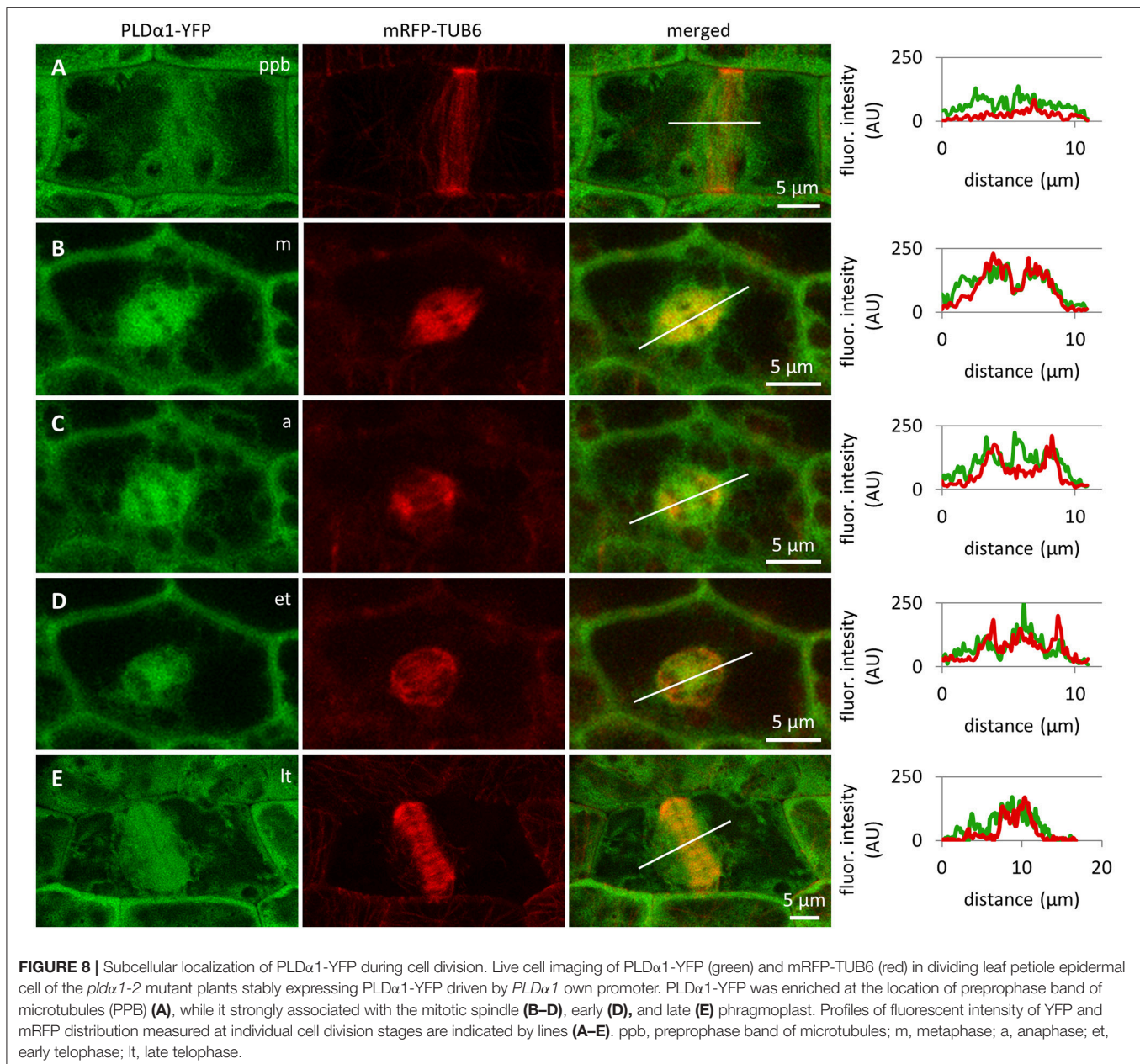


**FIGURE 7 |** Subcellular localization of PLD $\alpha$ 1-YFP and cortical microtubules in respect to the plasma membrane in leaf petiole epidermal cells of the *pld $\alpha$ 1-2* mutant plants stably expressing PLD $\alpha$ 1-YFP driven by *PLD $\alpha$ 1* own promoter. Living interphase petiole cells with the expression of PLD $\alpha$ 1-YFP (in green) and mRFP-TUB6 (in red) were counterstained with FM4-64 for delineation of the plasma membrane (in blue). **(A)** Orthogonal view of the 3D-reconstructed petiole cell from the z-stack imaging showing localization of plasma membrane, cortical microtubules and PLD $\alpha$ 1. Line in merged image indicates position of measured profile. **(B)** Profile intensity of fluorescence distribution of the plasma membrane (blue), cortical microtubules (red) and PLD $\alpha$ 1 (green) based on the distance from the cell surface. **(C)** Frontal view reconstructed from the individual z-stacks starting from the cell surface of the petiole cell to the cortical cytoplasm in steps indicating thickness of individual optical sections in  $\mu$ m. Individual channels are shown separately for the plasma membrane (labeled in blue), cortical microtubules (labeled in red) and PLD $\alpha$ 1 (labeled in green), while the merge image shows the overlay of all three channels with the depth annotation. **(D)** Maximum intensity projection of the same image as in C from the side view (orthogonal projection) with the line indicating position of measured profile. **(E)** Profile intensity of fluorescence distribution of the plasma membrane (blue), cortical microtubules (red) and PLD $\alpha$ 1 (green) from **(D)** based on the distance from the cell surface. Analysis made in confocal microscope.



at later stages of the phragmoplast expansion (Figure 10C, Video S3). During phragmoplast enlargement to the cell edges and consolidation of newly formed daughter nuclei, PLD $\alpha$ 1-YFP appeared to be more accumulated in the developing cell plate (Figure 10D). These results are consistent with PLD $\alpha$ 1-YFP accumulation within and around mitotic microtubule arrays during cell division observed by live cell imaging (Figure 8).

Next, we employed immunofluorescence localization of tubulin in dividing and non-dividing interphase cells of primary roots of *pld $\alpha$ 1-1* mutant to characterize possible involvement of PLD $\alpha$ 1 on general microtubule organization (Figure S7). However, no obvious differences in the microtubule organization were observed during mitosis, cytokinesis or in non-dividing

interphase cells of *pld $\alpha$ 1-1* mutant in comparison to wild type Col-0 plants (Figure S7).

### Association of PLD $\alpha$ 1-YFP With Microtubules and CCVs and CCPs

In order to address the functional relationship between mitotic microtubules and PLD $\alpha$ 1 in vesicular trafficking, we performed immunofluorescence localization of PLD $\alpha$ 1-YFP with microtubules and CCVs and CCPs in dividing and non-dividing rhizodermal cells of complemented *pld $\alpha$ 1-1* mutant seedlings expressing *proPLD $\alpha$ 1::PLD $\alpha$ 1:YFP* construct (Figure S8). In cytokinetic cells, PLD $\alpha$ 1-YFP was associated with microtubules of the ring phragmoplast, while signal was less abundant in the

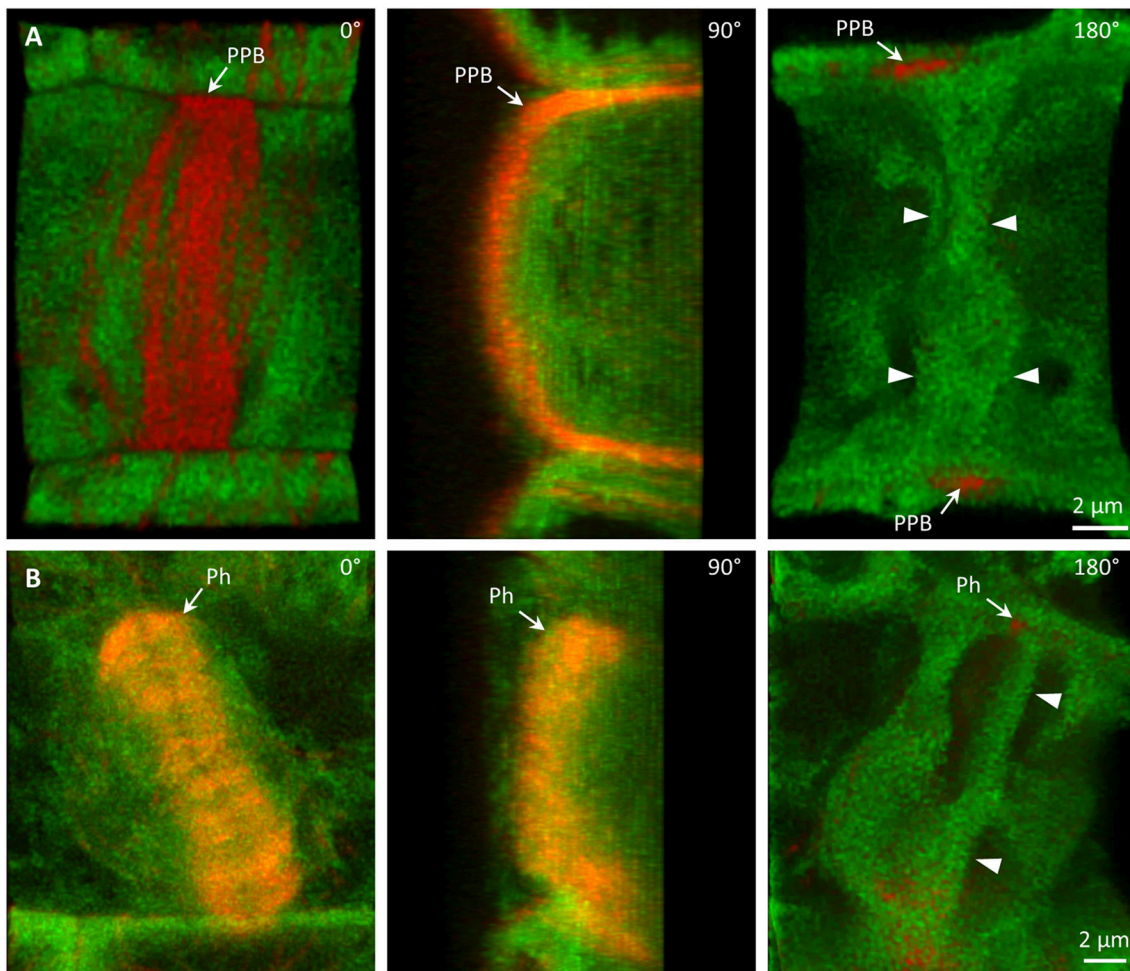


**FIGURE 9** | Association of PLD $\alpha$ 1-YFP with microtubules during cell division. Live cell imaging of dividing leaf epidermal petiole cells of complemented *pld $\alpha$ 1-2* mutant seedlings expressing PLD $\alpha$ 1-YFP and mRFP-TUB6. **(A)** Rotation of 3-D reconstructed pre-prophase cell with established PPB (arrows) showing localization of PLD $\alpha$ 1-YFP in cytoplasmic disk between cell nucleus and cortical PPB zone (arrowheads). Individual positions of rotating orthogonal projection correspond to **Video S1**. **(B)** Rotation of 3-D reconstructed cytokinetic cell with ring phragmoplast (Ph, arrows) showing localization of PLD $\alpha$ 1-YFP among phragmoplast microtubules, in cytoplasm around the phragmoplast and in emerging cell plate in the central zone of the ring phragmoplast (arrowheads). Individual positions of rotating orthogonal projection correspond to **Video S2**.

phragmoplast central part. The distribution of clathrin signal in this zone was complementary to PLD $\alpha$ 1-YFP distribution, with increased abundance in the central part and decreased abundance at the zone of phragmoplast microtubules (**Figure S8A**). Thus, the highest overlap of the clathrin and the PLD $\alpha$ 1-YFP signal was observed at the trailing (inner) edge of the enlarging phragmoplast (**Figure S8A**).

In non-dividing rhizodermal cells cortical microtubules were bedecked with PLD $\alpha$ 1-YFP closely associated or partially colocalizing with CCVs. PLD $\alpha$ 1-YFP was localized in spot-like structures decorating surface of microtubules in close association or partial colocalization with CCVs (**Figure S8B**). For more detailed subcellular study of PLD $\alpha$ 1 and microtubules involvement in vesicular trafficking we used super-resolved structural illumination microscopy (SIM). This analysis revealed association and partial colocalization of PLD $\alpha$ 1-YFP with CCVs and CCPs in the close vicinity of cortical microtubules, in

some cases creating spots and ring-like structures on their surface (**Figure 11A**). Association of PLD $\alpha$ 1-YFP with CCVs and CCPs in the cytoplasm between cortical microtubules was observed in clathrin-rich clusters that were in close contact with cortical microtubules (**Figure 11B**). Quantitative analysis of the above colocalization studies of clathrin and microtubules following either SIM or CLSM documentation, showed positive colocalization in Col-0 rhizodermal cells (Pearson's coefficient  $R = 0,62$ ) and no colocalization in *pld $\alpha$ 1* mutant (Pearson's coefficient  $R = 0$ ). In conclusion, these data document a complex pattern of PLD $\alpha$ 1 subcellular localization and its functional relationship to microtubule arrays in both non-dividing and dividing cells of Arabidopsis plants. Combination of different advanced microscopy methods provided data supporting a possible mechanism of interactions between clathrin-dependent endocytosis and cortical (as well as mitotic) microtubules, through the stabilization function of the PLD $\alpha$ 1.

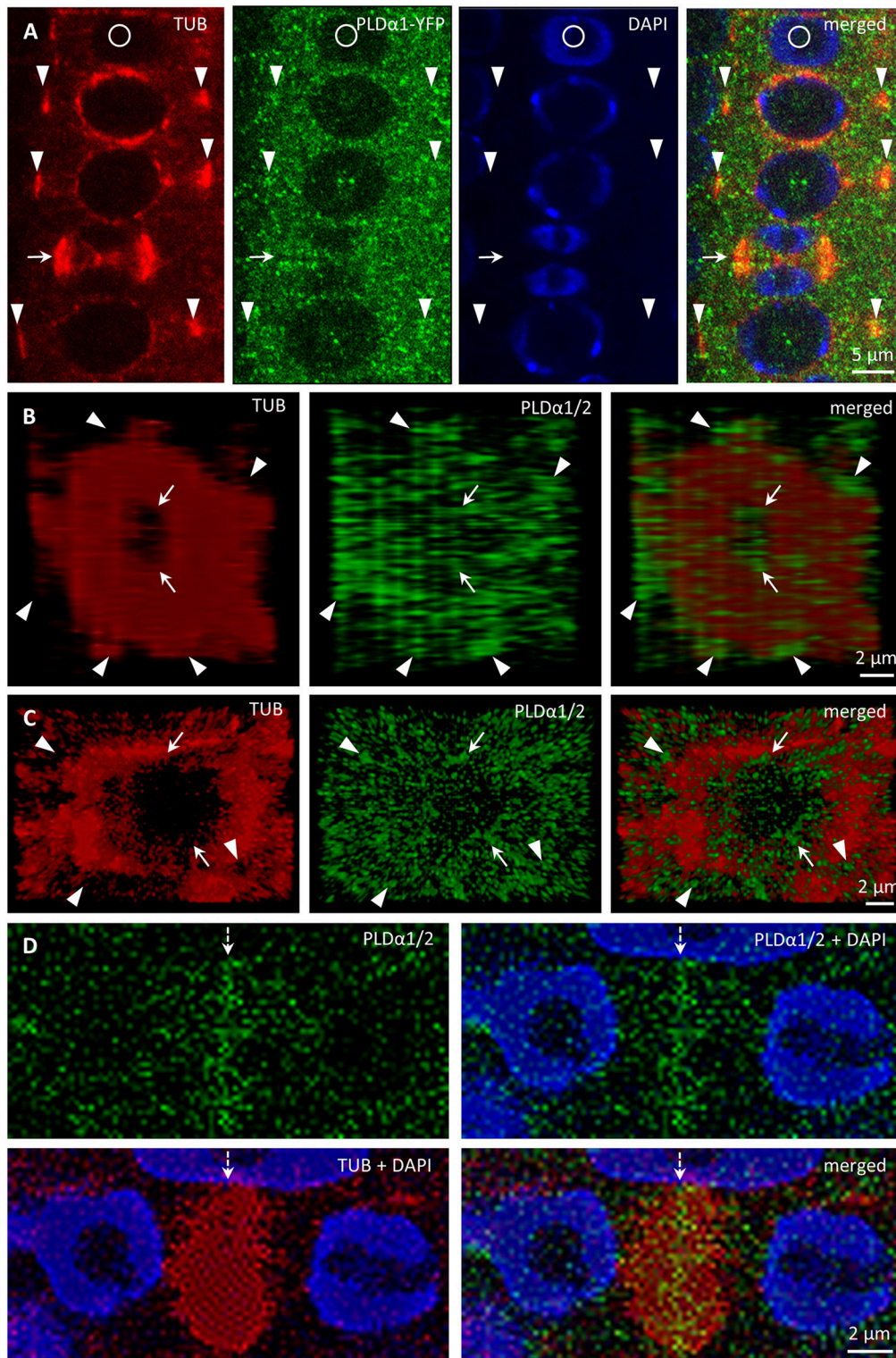


**FIGURE 10 |** Immunofluorescence colocalization of microtubules and PLD $\alpha$ 1-YFP during cell division in Arabidopsis root meristem cells of complemented *pld $\alpha$ 1-1* mutant seedlings expressing PLD $\alpha$ 1-YFP. **(A)** Colocalization of PLD $\alpha$ 1-YFP with microtubules of PPB (arrowheads) and late phragmoplast (arrow). Note that circle indicates non-dividing cell. **(B)** Orthogonal projection of disk phragmoplast stage with the distribution of PLD $\alpha$ 1-YFP at the leading (outer) edge (arrowheads) as well as at the trailing (inner) edge in the central part (arrows) of the phragmoplast. Still image of the orthogonal projection corresponds to **Video S3**. **(C)** Orthogonal projection of more advanced ring phragmoplast showing association of PLD $\alpha$ 1-YFP with the leading edge (arrowheads) and the trailing edge (arrows) of the phragmoplast. Still image of the orthogonal projection corresponds to **Video S4**. **(D)** Accumulation of PLD $\alpha$ 1-YFP in central part of the phragmoplast (arrow) at later stages of cytokinesis.

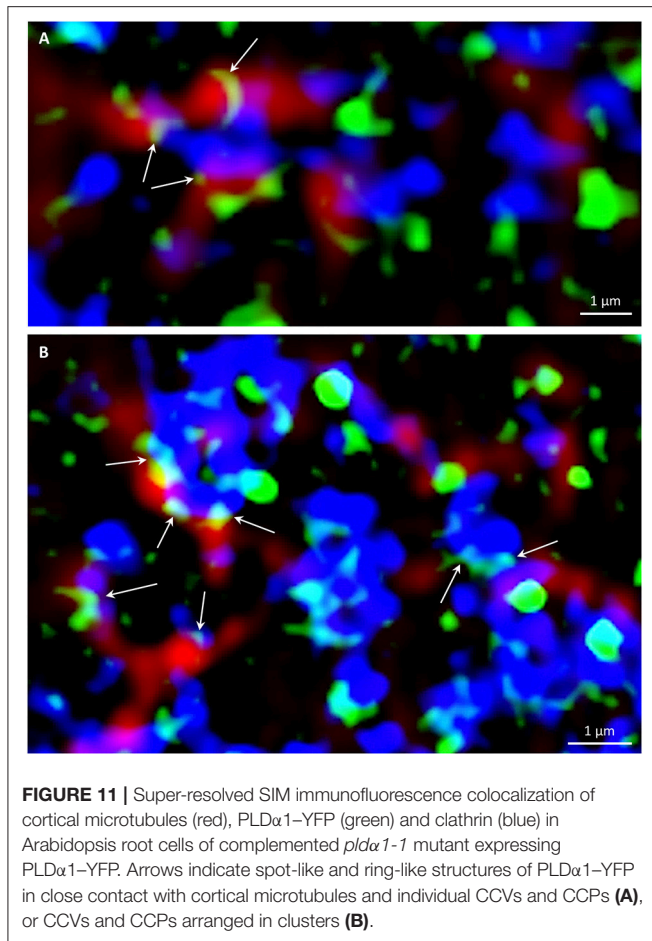


**FIGURE 11 |** Super-resolved SIM immunofluorescence colocalization of cortical microtubules (red), PLD $\alpha$ 1-YFP (green) and clathrin (blue) in Arabidopsis root cells of complemented *pld $\alpha$ 1-1* mutant expressing PLD $\alpha$ 1-YFP. Arrows indicate spot-like and ring-like structures of PLD $\alpha$ 1-YFP in close contact with cortical microtubules and individual CCVs and CCPs (A), or CCVs and CCPs arranged in clusters (B).

Finally, we wanted to test whether stress factors such as high salinity can induce subcellular relocation of PLD $\alpha$ 1-YFP in Arabidopsis cells. Indeed, PLD $\alpha$ 1-YFP was relocated and accumulated in curved surface areas of plasmolysed protoplasts of hypocotyl cells treated with 500 mM NaCl (Figure 12). These data suggest a possible protective role of PLD $\alpha$ 1 in these curved areas of retracting protoplasts detached from the cell wall during plasmolysis.

## DISCUSSION

The most prominent phospholipid-hydrolyzing enzymes in plants are members of phospholipase D (PLD) family. *A. thaliana* PLD $\alpha$ 1 and its product phosphatidic acid (PA) are closely associated with a wide range of cellular and physiological functions, such as regulation of stomatal closure and opening, cytoskeletal reorganization and stress signaling (Qin et al., 1997; Zhang et al., 2004; Bargmann and Munnik, 2006; Pleskot et al., 2013; Hong et al., 2016). Here we employed advanced microscopic methods to reveal precise developmental expression pattern and subcellular localization of PLD $\alpha$ 1 in two rescued *pld $\alpha$ 1* mutant lines.

ABA is an important hormone that regulates the adaptation of plants to various abiotic stresses (Danquah et al., 2014).

It was shown by previous studies that *pld $\alpha$ 1* mutant plants did not exhibit significant differences in morphological and developmental characteristics as compared to wild type plants (Fan et al., 1997; Zhang et al., 2012). However, PLD $\alpha$ 1 controls proper water balance in plant responding to ABA hormone by stomatal closure which was impaired in *pld $\alpha$ 1* knockout mutants (Zhang et al., 2004; Guo et al., 2012; Jiang et al., 2014). Here we transformed *pld $\alpha$ 1-1* and *pld $\alpha$ 1-2* mutant plants with *proPLD $\alpha$ ::PLD $\alpha$ 1-YFP* construct and we observed stomatal closure after ABA treatment similar to the wild type, suggesting functional complementation of both mutants by this construct.

## Developmental Expression Pattern and Localization of PLD $\alpha$ 1-YFP

A previous study assessing organ distribution of PLD $\alpha$ 1 protein in Arabidopsis plants by immunoblotting analysis showed higher amounts of this protein in stems, flowers, roots, siliques, and old leaves. Moreover, the highest activity of PLD $\alpha$ 1 was found in soluble fractions isolated from roots, flowers, and siliques (Fan et al., 1999). This study, however, lacked cellular resolution within these organs. In contrast, advanced microscopy imaging used in our experiments revealed high expression levels of PLD $\alpha$ 1-YFP in the apical and lateral root cap cells. These findings were in agreement with absolute expression levels of PLD $\alpha$ 1 transcript from Genevestigator transcriptomic data (Brady et al., 2007). High expression levels of PLD $\alpha$ 1-YFP were found also in trichoblast cell files and in developing roots hairs suggesting its role during root hair development. These results are consistent with work of Potocký et al. (2014) reporting PA localization in the plasma membrane of tip-growing pollen tubes. In the aerial part of the plant we observed high PLD $\alpha$ 1-YFP protein signal in pavement and stomata guard cells, which is again in accordance to Genevestigator transcriptomic data (Yang et al., 2008). On the other hand, and contrary to Genevestigator transcriptomic data (Marks et al., 2009), we observed high expression levels of PLD $\alpha$ 1-YFP in developing trichomes. These results support the role of PLD $\alpha$ 1 protein in cell developmental processes and polar cell growth.

## Cytoplasmic Localization of PLD $\alpha$ 1-YFP

The subcellular distribution of PLD $\alpha$ 1 based on immunoblotting analyses of fractionated extracts of Arabidopsis leaves revealed the highest content at the plasma membrane, CCVs, intracellular membranes and mitochondria while only a small amount of protein was detected in nuclei (Fan et al., 1999).

Previously, it was reported that activation of PLD leads to rearrangement of cortical microtubules in suspension BY-2 cells (Dhonukshe et al., 2003). Later it was shown that PLD $\delta$  is the cortical microtubule-binding protein (Andreeva et al., 2009; Ho et al., 2009). Moreover, a current study revealed colocalization of the PLD $\delta$  with cortical microtubules near to the plasma membrane in the hypocotyl cells of Arabidopsis (Zhang et al., 2017b). Microtubule dynamics controls important processes such as mitosis, cytokinesis, cell elongation, and signal transduction (Wymer and Lloyd, 1996; Hashimoto and Kato, 2006; Jiang et al., 2014). Under normal conditions, knockout mutant *pld $\alpha$ 1* showed



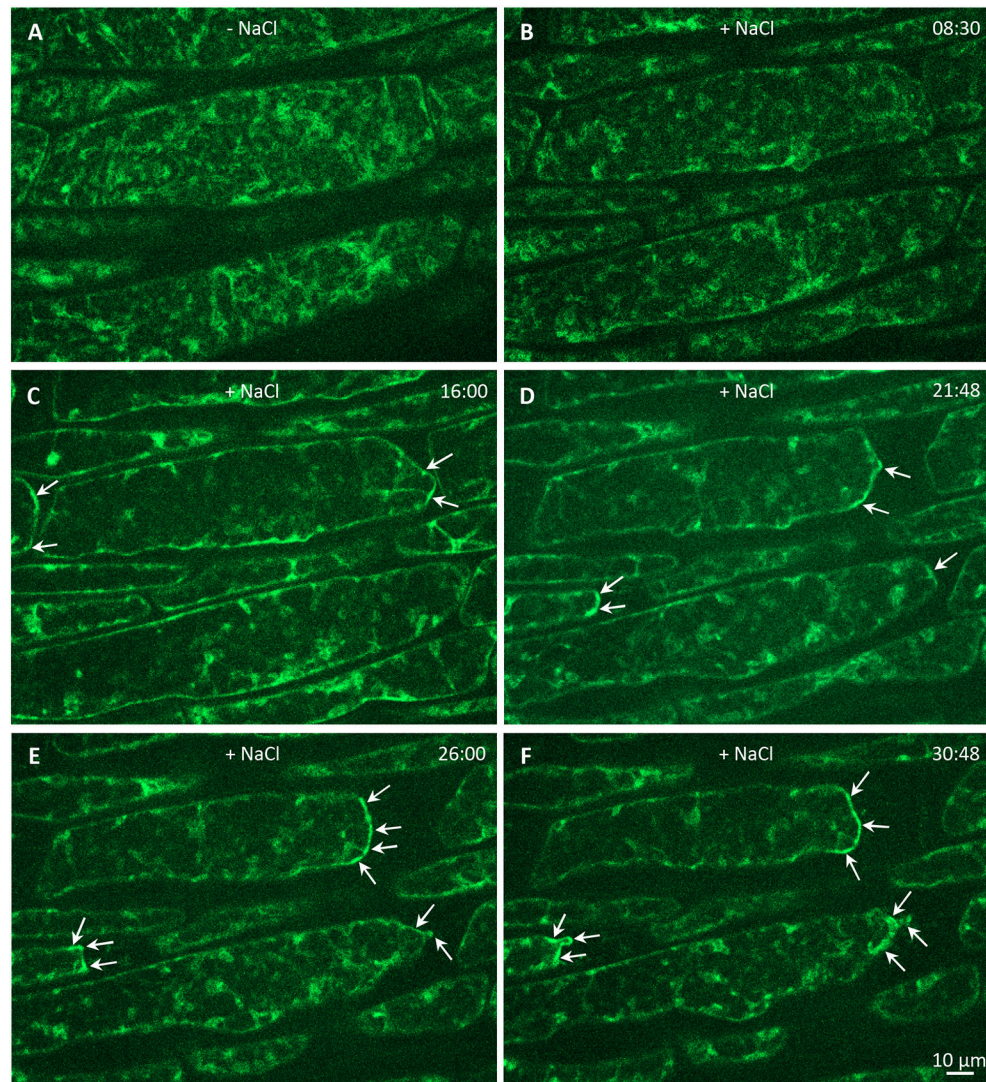


**FIGURE 12 |** Effect of salt stress on relocalization of PLD $\alpha$ 1-YFP (shown in artificial green color) driven by its native promoter in hypocotyl epidermal cells of complemented *pld $\alpha$ 1-2* mutant. **(A)** Time-lapse imaging of PLD $\alpha$ 1-YFP in hypocotyl epidermal cells under control conditions without salt and **(B–F)** during plasmolysis induced by 500 mM NaCl. The dynamic relocation and accumulation of PLD $\alpha$ 1-YFP in plasmolyzed surface areas of detaching protoplasts is depicted by arrows. Time is indicated in min:sec.

no changes in microtubule organization and density as compared to wild type plants (Zhang et al., 2012). However, PLD $\alpha$ 1 knockout in *Arabidopsis* leads to more severe disruption of cortical microtubules by inhibitors (Zhang et al., 2017a) or under salt stress conditions (Zhang et al., 2012). Furthermore, under the salt stress conditions PLD $\alpha$ 1 is activated and produce PA which directs AtMAP65-1 to the plasma membrane, leading to microtubule stabilization and enhanced cell protection (Zhang et al., 2012; Pleskot et al., 2014).

PLD $\alpha$ 1 is localized in both soluble and membrane fractions. It can translocate from cytosolic to membrane fractions and perform hydrolysis of membrane lipids under stress conditions (Wang et al., 2000; Hong et al., 2016). In our study we observed mainly cytoplasmic localization of PLD $\alpha$ 1-YFP, sometimes in

the vicinity of cortical microtubules, in non-dividing cells. By contrast, the localization of PLD $\delta$  which interacts with cortical microtubules was primarily restricted to the plasma membrane (Zhang et al., 2017b). With the entering of the cell to the mitosis PLD $\alpha$ 1-YFP was enriched at mitotic microtubule arrays, namely PPB, microtubules of mitotic spindle in prophase, metaphase and anaphase, as well as to microtubules of the phragmoplast during cytokinesis. Although, colocalization between PLD $\alpha$ 1 protein and microtubules was not previously observed in non-dividing protoplasts (Zhang et al., 2012), we detected accumulation of PLD $\alpha$ 1-YFP at microtubule arrays during mitotic progression. These results were further confirmed using immunofluorescence colocalization of PLD $\alpha$ 1-YFP and microtubules. PLD $\alpha$ 1-YFP protein was slightly accumulated and partially colocalized with

microtubules of preprophase band, spindle, and both early and late phragmoplast.

Multiple PLDs have been implicated to have redundant roles in ABA signaling and hyperosmotic stress. However, their mechanisms of action might be different. Single knockouts of either *PLD $\alpha$ 1* or *PLD $\delta$*  cause the inhibition of ABA-induced stomatal closure while stomata of double mutant are almost completely insensitive to ABA (Zhang et al., 2004; Guo et al., 2012; Uraji et al., 2012; Hong et al., 2016). Moreover, *PLD $\alpha$ 1*, through PA as an intermediate, promotes  $H_2O_2$  production, whereas *PLD $\delta$*  mediates the response to  $H_2O_2$  in the ABA signaling pathway. In this scenario *PLD $\alpha$ 1* can indirectly regulate *PLD $\delta$*  activity through ROS production (Guo et al., 2012; Hong et al., 2016). Gh*PLD $\alpha$ 1* and  $H_2O_2$  in the upland cotton (*Gossypium hirsutum*) are important components during the onset of the secondary cell wall thickening suggesting a putative role of *PLD $\alpha$ 1* in the vesicle trafficking (Tang and Liu, 2017). Furthermore, *PLD $\alpha$ 1* produced PA directs AtMAP65-1 to the plasma membrane and enhances its microtubule stabilizing activity, thus microtubules are stabilized and cell survival is enhanced under salt stress conditions (Zhang et al., 2012; Pleskot et al., 2014). Based on these findings, the question is posed whether *PLD $\alpha$ 1* can regulate mitotic progress alone or through PA, e.g., through the interaction with e.g., MAP65 proteins and/or *PLD $\delta$*  protein. More experiments should be performed to clarify the molecular mechanism by which *PLD $\alpha$ 1* affects mitotic microtubule arrays.

In mammals, PLD-PA signaling complexes regulate protein-membrane and membrane-cytoskeleton interactions, as well as vesicle budding and trafficking including exocytosis and endocytosis (McMahon and Gallop, 2005; Donaldson, 2009). Vesicle coating proteins, ARFs, Rho GTPases and soluble N-ethylmaleimide-sensitive factor attachment receptor (SNARE) proteins can interact with PLD and/or PA during vesicle formation at donor membranes, transport, docking, and fusion of vesicles with the target membranes (Chernomordik and Kozlov, 2003; Donaldson, 2009). In plants, there is some evidence that ARFs, Rho GTPases, SNARE proteins and PLDs are involved in vesicle targeting to the cell division plane, vesicle fusion, and cell plate biogenesis, although the exact roles of particular signaling proteins remains elusive (Zárský et al., 2009; El Kasmi et al., 2013; Smertenko et al., 2017).

Spo14 is phospholipase D of *Saccharomyces cerevisiae*, which specifically hydrolyzes phosphatidylcholine to generate choline and PA. Spo14p is localized to the cytoplasm of vegetative cells, however, it relocates to the spindle pole bodies and prospore membrane during sporulation (Rudge et al., 1998; Liu et al., 2007). PA produced by Spo14p is required to localize t-SNARE protein Spo20p to the prospore membrane (Nakanishi et al., 2006; Liu et al., 2007). As mentioned above, *PLD $\alpha$ 1* was enriched in the CCVs predicting its role in vesicular trafficking (Fan et al., 1999). Furthermore, AP180 (N-terminal homology domain clathrin-assembly) proteins and clathrins were identified as PA binding proteins in a previous proteomic study (McLoughlin et al., 2013). Similarly, epsin-like clathrin adaptor 1 binds PA under the negative membrane curvature stress in *Arabidopsis* (Putta et al., 2016). Furthermore, *PLD $\alpha$ 1* coimmunoprecipitates

with *Arabidopsis* AP-2 complex and clathrin (Yamaoka et al., 2013), indicating that *PLD $\alpha$ 1* contributes to clathrin-mediated endocytosis. These data indicate that proteins involved in the clathrin-dependent endocytosis are potential targets of *PLD $\alpha$ 1*-generated PA. Here we provide evidence for close associations of *PLD $\alpha$ 1*-YFP with cortical and mitotic microtubules during cell division. It has been shown previously that the PPB region at the cell cortex possess a large number of CCPs and CCVs. Expected role of clathrin-mediated endocytosis in the PPB area is related to the regulated modification of the cell cortex by controlled removal of particular membrane proteins by endocytosis, being part of the cell division plane memory establishment (Karahara et al., 2009). Centrifugal expansion of the phragmoplast during cytokinesis is driven by microtubule polymerization with substantial microtubule stabilization by bundling at the leading edge of the phragmoplast (Murata et al., 2013). Phragmoplast microtubules are responsible for delivery of vesicles creating cell plate in the mid-zone region. Cell plate formation, however, is also based on removal of excess membrane and cell wall material. Endocytosis and membrane recycling thus play an indispensable role during cell plate expansion (van Oostende-Triplet et al., 2017). Endocytosis was implicated in the spatial restriction of syntaxin protein KNOLLE to the cell plate (Boutté et al., 2010) and in the removal of the cellulose synthase enzymes from the central part and their recycling to the peripheral growth zone of the cell plate (Miart et al., 2014). Consistently with these observations electron tomography analysis revealed a high density of CCPs and CCVs during the transformation of the tubulo-vesicular network to a planar fenestrated sheet during cell plate formation (Seguí-Simarro et al., 2004). CCPs and CCVs were mostly localized at the trailing (inner) edge of the enlarging phragmoplast. Internalization and recycling of material from the central part and its delivery to the leading edges of maturing cell plate were thus definitely connected to clathrin-dependent endocytosis (Boutté et al., 2010; Ito et al., 2012; Teh et al., 2013; Miart et al., 2014). Based on these findings and on our results we suggest that *PLD $\alpha$ 1* and its product PA might participate in the complex signaling network involved in the vesicle trafficking and membrane assembly during plant cytokinesis. Although the precise mechanism by which *PLD $\alpha$ 1* or PA are involved in these processes is unknown, our results indicate that *PLD $\alpha$ 1* localized on microtubule surface can potentially functions as molecular glue for CCPs and CCVs associated with microtubules. This is further corroborated by the observation that microtubule-colocalized clathrin structures are quantitatively absent in the *pld $\alpha$ 1* mutant.

In animal literature it is suggested that PLD and PA participate in vesicle formation at various cellular membranes. One possible mechanism is that physiochemical properties of PLD and PA as well as their protein-protein and lipid-protein interactions (e.g., with dynamin, COPI, kinesin, ARF, small GTPases, phosphatases, kinases, and phosphoinositols) might regulate such vesicle formation (Manifava et al., 2001; Roth, 2008; Brito de Souza et al., 2014). More physiological and functional studies will be needed to prove this concept experimentally. But complex pattern of *PLD $\alpha$ 1* developmental expression, subcellular localization, and

its close association with cortical and mitotic microtubules in *Arabidopsis* documented here by advanced microscopy methods substantially contribute to this scenario and will promote further research in this topic.

## AUTHOR CONTRIBUTIONS

DN, PV, MO, OŠ, and JC: Conducted experiments; DN, MO, and OŠ: made image post acquisition analyses; GK: Helped with quantitative evaluations and data interpretation; PV, DN, MO, OŠ, and JŠ: Wrote the manuscript with input from all co-authors; JŠ: Proposed experiments and supervised this study, participated on data interpretation and finalized manuscript.

## FUNDING

This work was supported by the Czech Science Foundation GACR, grant Nr. 16-22044S.

## ACKNOWLEDGMENTS

We thank professor Geoffrey O. Wasteneys for *Arabidopsis* seeds carrying *pUBQ1:mRFP::TUB6* construct.

## SUPPLEMENTARY MATERIAL

The Supplementary Material for this article can be found online at: <https://www.frontiersin.org/articles/10.3389/fpls.2018.00371/full#supplementary-material>

**Figure S1** | Comparison of PLD $\alpha$ 1-YFP localization in different aerial organs and tissues of *pld $\alpha$ 1-1* (A–E) and *pld $\alpha$ 1-2* (F–J) mutants stably expressing PLD $\alpha$ 1-YFP driven by its own promoter: epidermis of first true leaf (A,F), epidermal cells of hypocotyl (B,G), epidermal cells of cotyledon petiole (C,H), epidermal cells of cotyledon (D,I) and entire 5 days-old seedling (E,J).

**Figure S2** | PLD $\alpha$ 1-YFP localization in different tissues of the root tip of rescued *pld $\alpha$ 1-1* mutant stably transformed with *proPLD $\alpha$ 1::PLD $\alpha$ 1:YFP* construct by light-sheet fluorescence microscopy. (A) Localization of PLD $\alpha$ 1-YFP in cells of the root tip counterstained by propidium iodide and merged image. Profiles at different

positions of the root tip are visualized in orthogonal projections of radial root sections in (B).

**Figure S3** | PLD $\alpha$ 1-YFP localization in different tissues of the root tip of rescued *pld $\alpha$ 1-2* mutant stably transformed with *proPLD $\alpha$ 1::PLD $\alpha$ 1:YFP* construct by light-sheet fluorescence microscopy. (A) Localization of PLD $\alpha$ 1-YFP in cells of the root tip counterstained by propidium iodide and merged image. Profiles at different positions of the root tip are visualized in orthogonal projections of radial root sections in (B).

**Figure S4** | PLD $\alpha$ 1-YFP localization in trichoblast (labeled as T) and atrichoblast (labeled as A) rhizodermis cell files of the root tip of rescued *pld $\alpha$ 1-1* mutant stably transformed with *proPLD $\alpha$ 1::PLD $\alpha$ 1:YFP* construct by light-sheet fluorescence microscopy. Localization of PLD $\alpha$ 1-YFP, propidium iodide and merged image of the root transition zone in longitudinal (A) and transversal (B) root projections.

**Figure S5** | PLD $\alpha$ 1-YFP localization in trichoblast (labeled as T) and atrichoblast (labeled as A) rhizodermis cell files of the root tip of rescued *pld $\alpha$ 1-2* mutant stably transformed with *proPLD $\alpha$ 1::PLD $\alpha$ 1:YFP* construct by light-sheet fluorescence microscopy. Localization of PLD $\alpha$ 1-YFP, propidium iodide and merged image of the root transition zone in longitudinal (A) and transversal (B) root projections.

**Figure S6** | Immunofluorescence localization of PLD $\alpha$ 1 protein in *Arabidopsis* root meristem cells of wild type Col-0 seedlings showing homogeneous distribution of PLD $\alpha$ 1 in the cytoplasm.

**Figure S7** | Organization of microtubule arrays in dividing cells of root meristem in *pld $\alpha$ 1-1* mutant in comparison to wild type Col-0. Arrowheads indicate PPBs, red arrows mitotic spindles and white arrows phragmoplasts. Immunofluorescence localization of microtubules with confocal microscopy, nuclei are counterstained with DAPI.

**Figure S8** | Immunofluorescence colocalization of microtubules with PLD $\alpha$ 1-YFP and clathrin in *Arabidopsis* root cells of complemented *pld $\alpha$ 1-1* mutant expressing PLD $\alpha$ 1-YFP. (A) Colocalization of microtubules (green), PLD $\alpha$ 1-YFP (red), and clathrin (blue) in late phragmoplast of root meristematic cell during the cytokinesis. (B) Colocalization of cortical microtubules (green), PLD $\alpha$ 1-YFP (blue) and clathrin (red) in interphase root cell. Boxed areas in (B) are magnified in (C). Arrows indicate colocalization of PLD $\alpha$ 1-YFP with clathrin in association with cortical microtubules.

**Video S1** | 3-D rendering of leaf epidermal petiole cell at the pre-prophase stage of cell division with established PPB and localization of PLD $\alpha$ 1-YFP.

**Video S2** | 3-D rendering of leaf epidermal petiole cell at the cytokinesis with ring phragmoplast and localization of PLD $\alpha$ 1-YFP.

**Video S3** | 3-D rendering of early disk phragmoplast in root meristematic cell at the cytokinesis with localization of PLD $\alpha$ 1-YFP.

**Video S4** | 3-D rendering of late ring phragmoplast in root meristematic cell at the cytokinesis with localization of PLD $\alpha$ 1-YFP.

## REFERENCES

- Ambrose, C., Allard, J. F., Cytrynbaum, E. N., and Wasteneys, G. O. (2011). A CLASP-modulated cell edge barrier mechanism drives cell-wide cortical microtubule organization in *Arabidopsis*. *Nat. Commun.* 16, 430. doi: 10.1038/ncomms1444
- Andreeva, Z., Ho, A. Y. Y., Barthelet, M. M., Potocký, M., Bezvoda, R., Žárský, V., et al. (2009). Phospholipase D family interactions with the cytoskeleton: isoform  $\delta$  promotes plasma membrane anchoring of cortical microtubules. *Funct. Plant Biol.* 36, 600–612. doi: 10.1071/FP09024
- Bargmann, B. O., and Munnik, T. (2006). The role of phospholipase D in plant stress responses. *Curr. Opin. Plant Biol.* 9, 515–522. doi: 10.1016/j.pbi.2006.07.011
- Bargmann, B. O., Laxalt, A. M., ter Riet, B., van Schooten, B., Merquiol, E., Testerink, C., et al. (2009). Multiple PLDs required for high salinity and water deficit tolerance in plants. *Plant Cell Physiol.* 50, 78–89. doi: 10.1093/pcp/pcn173
- Boutté, Y., Frescatada-Rosa, M., Men, S., Chow, C. M., Ebine, K., Gustavsson, A., et al. (2010). Endocytosis restricts *Arabidopsis* KNOLLE syntaxin to the cell division plane during late cytokinesis. *EMBO J.* 29, 546–558. doi: 10.1038/emboj.2009.363
- Brady, S. M., Orlando, D. A., Lee, J. Y., Wang, J. Y., Koch, J., Dinneny, J. R., et al. (2007). A high-resolution root spatiotemporal map reveals dominant expression patterns. *Science* 318, 801–806. doi: 10.1126/science.1146265
- Brito de Souza, L., Pinto da Silva, L. L., Jamur, M. C., and Oliver, C. (2014). Phospholipase D is involved in the formation of Golgi associated clathrin coated vesicles in human parotid duct cells. *PLoS ONE* 9:91868. doi: 10.1371/journal.pone.0091868
- Chernomordik, L. V., and Kozlov, M. M. (2003). Protein-lipid interplay in fusion and fission of biological membranes. *Annu. Rev. Biochem.* 72, 175–207. doi: 10.1146/annurev.biochem.72.121801.161504
- Choudhury, S. R., and Pandey, S. (2016). The role of PLD $\alpha$ 1 in providing specificity to signal-response coupling by heterotrimeric G-protein components in *Arabidopsis*. *Plant J.* 86, 50–61. doi: 10.1111/tbj.13151
- Choudhury, S. R., and Pandey, S. (2017). Phosphatidic acid binding inhibits RGS1 activity to affect specific signaling pathways in *Arabidopsis*. *Plant J.* 90, 466–477. doi: 10.1111/tbj.13503

- Clough, S. J., and Bent, A. F. (1998). Floral dip: a simplified method for *Agrobacterium*-mediated transformation of *Arabidopsis thaliana*. *Plant J.* 16, 735–743. doi: 10.1046/j.1365-313x.1998.00343.x
- Danquah, A., de Zelicourt, A., Colcombet, J., and Hirt, H. (2014). The role of ABA and MAPK signaling pathways in plant abiotic stress responses. *Biotechnol. Adv.* 32, 40–52. doi: 10.1016/j.biotechadv.2013.09.006
- Davis, A. M., Hall, A., Millar, A. J., Darrah, C., and Davis, S. J. (2009). Protocol: streamlined sub-protocols for floral-dip transformation and selection of transformants in *Arabidopsis thaliana*. *Plant Methods* 5:3. doi: 10.1186/1746-4811-5-3
- Dhonukshe, P., Laxalt, A. M., Goedhart, J., Gadella, T. W., and Munnik, T. (2003). Phospholipase d activation correlates with microtubule reorganization in living plant cells. *Plant Cell* 15, 2666–2679. doi: 10.1105/tpc.014977
- Donaldson, J. G. (2009). Phospholipase D in endocytosis and endosomal recycling pathways. *Biochim. Biophys. Acta* 1791, 845–849. doi: 10.1016/j.bbali.2009.05.011
- El Kasmi, F., Krause, C., Hiller, U., Stierhof, Y. D., Mayer, U., Conner, L., et al. (2013). SNARE complexes of different composition jointly mediate membrane fusion in *Arabidopsis* cytokinesis. *Mol. Biol. Cell* 24, 1593–1601. doi: 10.1091/mbc.E13-02-0074
- Fan, L., Zheng, S., and Wang, X. (1997). Antisense suppression of phospholipase D  $\alpha$  retards abscisic acid- and ethylene-promoted senescence of postharvest *Arabidopsis* leaves. *Plant Cell* 9, 2183–2196. doi: 10.1105/tpc.9.12.2183
- Fan, L., Zheng, S., Cui, D., and Wang, X. (1999). Subcellular distribution and tissue expression of phospholipase D $\alpha$ , D $\beta$ , and D $\gamma$  in *Arabidopsis*. *Plant Phys.* 119, 1371–1378. doi: 10.1104/pp.119.4.1371
- Gardiner, J. C., Harper, J. D., Weerakoon, N. D., Collings, D. A., Ritchie, S., Gilroy, S., et al. (2001). A 90-kD phospholipase D from tobacco binds to microtubules and the plasma membrane. *Plant Cell* 13, 2143–2158. doi: 10.1105/tpc.13.9.2143
- Guo, L., Mishra, G., Markham, J. E., Li, M., Tawfall, A., Welti, R., et al. (2012). Connections between sphingosine kinase and phospholipase D in the abscisic acid signaling pathway in *Arabidopsis*. *J. Biol. Chem.* 287, 8286–8296. doi: 10.1074/jbc.M111.274274
- Hashimoto, T., and Kato, T. (2006). Cortical control of plant microtubules. *Curr. Opin. Plant Biol.* 9, 5–11. doi: 10.1016/j.pbi.2005.11.005
- Ho, A. Y. Y., Day, D. A., Brown, M. H., and Marc, J. (2009). *Arabidopsis* phospholipase D $\delta$  as an initiator of cytoskeleton-mediated signalling to fundamental cellular processes. *Funct. Plant Biol.* 36, 190–198. doi: 10.1071/FP08222
- Hong, Y., Zhao, J., Guo, L., Kim, S. C., Deng, X., Wang, G., et al. (2016). Plant phospholipases D and C and their diverse functions in stress responses. *Prog. Lipid Res.* 62, 55–74. doi: 10.1016/j.plipres.2016.01.002
- Ito, E., Fujimoto, M., Ebine, K., Uemura, T., Ueda, T., and Nakano, A. (2012). Dynamic behavior of clathrin in *Arabidopsis thaliana* unveiled by live imaging. *Plant J.* 69, 204–216. doi: 10.1111/j.1365-313X.2011.04782.x
- Jiang, Y., Wu, K., Lin, F., Qu, Y., Liu, X., and Zhang, Q. (2014). Phosphatidic acid integrates calcium signaling and microtubule dynamics into regulating ABA-induced stomatal closure in *Arabidopsis*. *Planta* 239, 565–575. doi: 10.1007/s00425-013-1999-5
- Karahara, L., Suda, J., Tahara, H., Yokota, E., Shimmen, T., Misaki, K., et al. (2009). The preprophase band is a localized center of clathrin-mediated endocytosis in late prophase cells of the onion cotyledon epidermis. *Plant J.* 57, 819–831. doi: 10.1111/j.1365-313X.2008.03725.x
- Komis, G., Mistrik, M., Šamajová, O., and Ovečka, M., Bartek, J., and Šamaj, J. (2015). Superresolution live imaging of plant cells using structured illumination microscopy. *Nat. Protoc.* 10, 1248–1263. doi: 10.1038/nprot.2015.083
- Liu, S., Wilson, K. A., Rice-Stitt, T., Neiman, A. M., and McNew, J. A. (2007). *In vitro* fusion catalyzed by the sporulation-specific t-SNARE light-chain Spo20p is stimulated by phosphatidic acid. *Traffic* 8, 1630–1643. doi: 10.1111/j.1600-0854.2007.00628.x
- Manifava, M., Thuring, J. W., Lim, Z. Y., Packman, L., Holmes, A. B., and Ktistakis, N. T. (2001). Differential binding of traffic-related proteins to phosphatidic acid- or phosphatidylinositol (4,5)- bisphosphate-coupled affinity reagents. *J. Biol. Chem.* 276, 8987–8994. doi: 10.1074/jbc.M010308200
- Marks, M. D., Wenger, J. P., Gilding, E., Jilk, R., and Dixon, R. A. (2009). Transcriptome analysis of *Arabidopsis* wild-type and gl3-sst sim trichomes identifies four additional genes required for trichome development. *Mol. Plant* 2, 803–822. doi: 10.1093/mp/ssp037
- McLoughlin, F., Arisz, S. A., Dekker, H. L., Kramer, G., de Koster, C. G., Haring, M. A., et al. (2013). Identification of novel candidate phosphatidic acid-binding proteins involved in the salt-stress response of *Arabidopsis thaliana* roots. *Biochem. J.* 450, 573–581. doi: 10.1042/BJ20121639
- McMahon, H. T., and Gallop, J. L. (2005). Membrane curvature and mechanisms of dynamic cell membrane remodelling. *Nature* 438, 590–596. doi: 10.1038/nature04396
- Miart, F., Desprez, T., Biot, E., Morin, H., Belcram, K., Höfte, H., et al. (2014). Spatio-temporal analysis of cellulose synthesis during cell plate formation in *Arabidopsis*. *Plant J.* 77, 71–84. doi: 10.1111/tpj.12362
- Munnik, T., and Musgrave, A. (2001). Phospholipid signaling in plants: holding on to Phospholipase D. *Sci. STKE*. 2001:42. doi: 10.1126/stke.2001.111.pe42
- Murashige, T., and Skoog, F. (1962). A revised medium for rapid growth and bioassays with tobacco tissue cultures. *Physiol. Plant.* 15, 473–497. doi: 10.1111/j.1399-3054.1962.tb08052.x
- Murata, T., Sano, T., Sasabe, M., Nonaka, S., Higashiyama, T., Hasezawa, S., et al. (2013). Mechanism of microtubule array expansion in the cytokinetic phragmoplast. *Nat. Commun.* 4, 1967. doi: 10.1038/ncomms2967
- Nakanishi, H., Morishita, M., Schwartz, C. L., Coluccio, A., Engebrecht, J., and Neiman, A. M. (2006). Phospholipase D and the SNARE Sso1p are necessary for vesicle fusion during sporulation in yeast. *J. Cell. Sci.* 119, 1406–1415. doi: 10.1242/jcs.02841
- Ovečka, M., Vaškebová, L., Komis, G., Luptovčíak, I., Smertenko, A., and Šamaj, J. (2015). Preparation of plants for developmental and cellular imaging by light-sheet microscopy. *Nat. Protoc.* 10, 1234–1247. doi: 10.1038/nprot.2015.081
- Pleskot, R., Li, J., Žárský, V., Potocký, M., and Staiger, C. J. (2013). Regulation of cytoskeletal dynamics by phospholipase D and phosphatidic acid. *Trends Plant Sci.* 18, 496–504. doi: 10.1016/j.tplants.2013.04.005
- Pleskot, R., Pejchar, P., Staiger, C. J., and Potocký, M. (2014). When fat is not bad: the regulation of actin dynamics by phospholipid signaling molecules. *Front. Plant Sci.* 5:5. doi: 10.3389/fpls.2014.00005
- Potocký, M., Pleskot, R., Pejchar, P., Vitale, N., Kost, B., and Žárský, V. (2014). Live-cell imaging of phosphatidic acid dynamics in pollen tubes visualized by Spo20p-derived biosensor. *New Phytol.* 203, 483–494. doi: 10.1111/nph.12814
- Putta, P., Rankenberg, J., Korver, R. A., van Wijk, R., Munnik, T., Testerink, C., et al. (2016). Phosphatidic acid binding proteins display differential binding as a function of membrane curvature stress and chemical properties. *Biochim. Biophys. Acta* 1858, 2709–2716. doi: 10.1016/j.bbamem.2016.07.014
- Qin, C., and Wang, X. (2002). The *Arabidopsis* phospholipase D family. Characterization of a calcium-independent and phosphatidylcholine-selective PLD zeta 1 with distinct regulatory domains. *Plant Physiol.* 128, 1057–1068. doi: 10.1104/pp.010928
- Qin, W., Pappan, K., and Wang, X. (1997). Cloning of PLD $\gamma$  and regulation of plant PLD $\gamma$ ,  $\beta$  and  $\alpha$  by polyphosphoinositides and calcium. *J. Biol. Chem.* 272, 28267–28273. doi: 10.1074/jbc.272.45.28267
- Rego, E. H., Shao, L., Macklin, J. J., Winoto, L., Johansson, G. A., Kamps-Hughes, N., et al. (2012). Nonlinear structured-illumination microscopy with a photoswitchable protein reveals cellular structures at 50-nm resolution. *Proc. Natl. Acad. Sci. U.S.A.* 109, 135–143. doi: 10.1073/pnas.1107547108
- Roth, M. G. (2008). Molecular mechanisms of PLD function in membrane traffic. *Traffic* 9, 1233–1239. doi: 10.1111/j.1600-0854.2008.00742.x
- Rudge, S. A., Morris, A. J., and Engebrecht, J. (1998). Relocalization of phospholipase D activity mediates membrane formation during meiosis. *J. Cell Biol.* 140, 81–90. doi: 10.1083/jcb.140.1.81
- Šamajová, O., Komis, G., and Šamaj, J. (2014). Immunofluorescent localization of MAPKs and colocalization with microtubules in *Arabidopsis* seedling whole-mount probes. *Methods Mol. Biol.* 1171, 107–115. doi: 10.1007/978-1-4939-0922-3\_9
- Seguí-Simarro, J. M., Austin, J. R., White, E. A., and Staehelin, L. A. (2004). Electron tomographic analysis of somatic cell plate formation in meristematic cells of *Arabidopsis* preserved by high-pressure freezing. *Plant Cell* 16, 836–856. doi: 10.1105/tpc.017749
- Smertenko, A., Assaad, F., Baluška, F., Bezanilla, M., Buschmann, H., Drakakaki, G., et al. (2017). Plant cytokinesis: terminology for structures and processes. *Trends Cell Biol.* 27, 885–894. doi: 10.1016/j.tcb.2017.08.008

- Takáč, T., Šamajová, O., Pechan, T., Luptovčiak, I., and Šamaj, J. (2017). Feedback microtubule control and microtubule-actin cross-talk in Arabidopsis revealed by integrative proteomic and cell biology analysis of KATANIN1 mutants. *Mol. Cell. Proteomics* 16, 1591–1609. doi: 10.1074/mcp.M117.068015
- Tang, K., and Liu, J. Y. (2017). Molecular characterization of GhPLD $\alpha$ 1 and its relationship with secondary cell wall thickening in cotton fibers. *Acta Biochim. Biophys. Sin.* 49, 33–43. doi: 10.1093/abbs/gmw113
- Teh, O. K., Shimono, Y., Shirakawa, M., Fukao, Y., Tamura, K., Shimada, T., et al. (2013). The AP-1  $\mu$  adaptin is required for KNOLLE localization at the cell plate to mediate cytokinesis in Arabidopsis. *Plant Cell Physiol.* 54, 838–847. doi: 10.1093/pcp/pct048
- Uraji, M., Katagiri, T., Okuma, E., Ye, W., Hossain, M. A., Masuda, C., et al. (2012). Cooperative function of PLD $\delta$  and PLD $\alpha$ 1 in abscisic acid-induced stomatal closure in Arabidopsis. *Plant Physiol.* 159, 450–460. doi: 10.1104/pp.112.195578
- van Oostende-Triplet, C., Guillet, D., Triplet, T., Pandzic, E., Wiseman, P. W., and Geitmann, A. (2017). Vesicle dynamics during plant cell cytokinesis reveals distinct developmental phases. *Plant Physiol.* 174, 1544–1558. doi: 10.1104/pp.17.00343
- Wang, C., Zien, C. A., Afithile, M., Welti, R., Hildebrand, D. F., and Wang, X. (2000). Involvement of phospholipase D in wound-induced accumulation of jasmonic acid in Arabidopsis. *Plant Cell* 12, 2237–2246. doi: 10.1105/tpc.12.11.2237
- Wang, G., Ryu, S., and Wang, X. (2012). Plant phospholipases: an overview. *Methods Mol. Biol.* 861, 123–137. doi: 10.1007/978-1-61779-600-5\_8
- Wang, X. (2005). Regulatory functions of phospholipase D and phosphatidic acid in plant growth, development, and stress responses. *Plant Physiol.* 139, 566–573. doi: 10.1104/pp.105.068809
- Wymer, C., and Lloyd, C. (1996). Dynamic microtubules: implications for cell wall patterns. *Trends Plant Sci.* 7, 222–228. doi: 10.1016/S1360-1385(96)86899-0
- Yamaoka, S., Shimono, Y., Shirakawa, M., Fukao, Y., Kawase, T., Hatsugai, N., et al. (2013). Identification and dynamics of Arabidopsis adaptor protein-2 complex and its involvement in floral organ development. *Plant Cell* 25, 2958–2969. doi: 10.1105/tpc.113.114082
- Yang, Y., Costa, A., Leonhardt, N., Siegel, R. S., and Schroeder, J. I. (2008). Isolation of a strong Arabidopsis guard cell promoter and its potential as a research tool. *Plant Methods* 4:6. doi: 10.1186/1746-4811-4-6
- Žárský, V., Cvrčková, F., Potocký, M., and Hála, M. (2009). Exocytosis and cell polarity in plants – exocyst and recycling domains. *New Phytol.* 183, 255–272. doi: 10.1111/j.1469-8137.2009.02880.x
- Zhang, Q., Lin, F., Mao, T., Nie, J., Yan, M., Yuan, M., et al. (2012). Phosphatidic acid regulates microtubule organization by interacting with MAP65-1 in response to salt stress in Arabidopsis. *Plant Cell* 24, 4555–4576. doi: 10.1105/tpc.112.104182
- Zhang, Q., Qu, Y., Wang, Q., Song, P., Wang, P., Jia, Q., et al. (2017a). Arabidopsis phospholipase D $\alpha$  1-derived phosphatidic acid regulates microtubule organization and cell development under microtubule-interacting drugs treatment. *J. Plant Res.* 130, 193–202. doi: 10.1007/s10265-016-0870-8
- Zhang, Q., Song, P., Qu, Y., Wang, P., Jia, Q., Guo, L., et al. (2017b). Phospholipase D $\delta$  negatively regulates plant thermotolerance by destabilizing cortical microtubules in Arabidopsis. *Plant Cell Environ.* 40, 2220–2235. doi: 10.1111/pce.13023
- Zhang, W., Qin, C., Zhao, J., and Wang, X. (2004). Phospholipase D  $\alpha$ 1-derived phosphatidic acid interacts with ABI1 phosphatase 2C and regulates abscisic acid signaling. *Proc. Natl. Acad. Sci. U.S.A.* 101, 9508–9513. doi: 10.1073/pnas.0402112101

**Conflict of Interest Statement:** The authors declare that the research was conducted in the absence of any commercial or financial relationships that could be construed as a potential conflict of interest.

Copyright © 2018 Novák, Vadovič, Ovečka, Šamajová, Komis, Colcombet and Šamaj. This is an open-access article distributed under the terms of the Creative Commons Attribution License (CC BY). The use, distribution or reproduction in other forums is permitted, provided the original author(s) and the copyright owner are credited and that the original publication in this journal is cited, in accordance with accepted academic practice. No use, distribution or reproduction is permitted which does not comply with these terms.